UNIVERSITA' POLITECNICA DELLE MARCHE

FACOLTA' DI INGEGNERIA

Corso di Laurea Magistrale in Biomedical Engineering

METROLOGICAL EVALUATION OF THE COMPRESSIVE SAMPLING APPROACH APPLIED TO ELECTRODERMAL ACTIVITY SIGNALS IN RESPONSE TO AUDIO STIMULI

Supervisor:

Prof. Susanna Spinsante

Co-Supervisor:

Prof. Stefania Cecchi

Author:

Federico Casaccia

A.A. **2019 / 2020**

ABSTRACT

The ElectroDermal Activity (EDA) signal, recorded as the electrical conductance between a pair of electrodes placed over a person's skin, and linked to a person's emotional arousal, consists of a tonic component superposed by multiple Skin Conductance Responses (SCRs). Each SCR, in turn, results from a corresponding SCR event which is not directly observable from the measured EDA signal although its informative content is very useful in a wide range of applications. Thus, several approaches have been proposed to extract the SCR events from the EDA signal, but the problem has not been solved yet.

In this work, the effectiveness of a Compressed sensing (CS)-based approach for the extraction of SCR events from EDA signals measured with a wrist-worn wearable device, has been investigated. Once the sparse SCR events signals have been extracted from real EDA signals acquired during a sound stimuli experiment, the SCR onsets detection accuracy of this CS-based approach has been assessed against more traditionally used methods. The attained results show that, overall, there are no relevant differences but a small overestimate in the number of detected SCR onsets with the proposed approach compared to the other strategies, demonstrating the goodness of this CS-based method.

TABLE OF CONTENTS

INTRODUCTION

The ElectroDermal Activity (EDA) signal is typically recorded as the electric conductance between a pair of electrodes placed over a person's skin, near high density regions of sweat glands such as the hand palm or the fingertips [1]. This signal can be seen as an electrical manifestation of the sympathetic innervation of the sweat glands [2]. The hypothesized connection between variations in a subject's skin conductance and psychological state has been confirmed at the beginning of the 21st century by means of a simultaneous analysis of brain function, using fMRI, and skin conduction, using EDA [3]. In the last decade, wearable devices, such as the Empatica E4 wristband [4], have given us the opportunity to measure the EDA signal non-invasively in a simple but effective way also outside a standard laboratory setting.

The EDA signal is characterized by two dominant components: a slowly varying Skin Conductance Level (SCL), also referred to as the tonic component or baseline, and a phasic component consisting of multiple Skin Conductance Responses (SCRs), each arising from a corresponding SCR event or neuron burst event [1]. Neuron burst events, or SCR events, are difficult to extract from an observed EDA signal for a number of reasons, such as potentially overlapping SCRs, a predominant SCL [5]. In recent years, various signal decomposition approaches have been proposed to overcome these difficulties [6],[7],[8] but the problem still remains.

Because of the intrinsic sparse nature of the SCR events signal and exploiting a novel tailored model for the baseline component, a Compressed Sensing (CS)-based decomposition approach could be the answer [1].

The aim of this thesis is to investigate the effectiveness of a CS-based approach for the extraction of SCR events from EDA signals measured with a wrist-worn wearable device, in non-ambulatory settings. To such an aim, the CS-based decomposition framework for EDA signals proposed by [1] and based on CVX [9] for the reconstruction is implemented in Matlab, improved with the addition of a post-processing step, and tested using a combination of both synthetically generated and experimentally acquired EDA data. The SCR onsets detection accuracy of this CS-based approach is then assessed against more traditionally used tools and approaches such as Ledalab standard trough-to-peak (TTP) analysis [10] and Pocket guide algorithm [11]. The attained results show that, overall, there are no relevant differences but a small overestimate in the number of detected SCR

onsets with the proposed CS-based approach compared to the other two approaches, demonstrating the goodness of such approach.

The thesis is organized into seven main Chapters. In the first Chapter, the EDA signal characteristics and the state of art analysis are presented. In the second Chapter, CS framework and in particular the approximately sparse signals recovery problem, is described. In the third Chapter, the device used to measure the EDA signal, the EDA signal model and CS-based decomposition implemented in Matlab, are described. Additionally, in this Chapter the experimental protocol for the EDA signal acquisition in response to audio stimuli is explained. The fourth Chapter, titled “Experiments”, provides detailed information about both synthetically generated and experimentally acquired EDA data. Moreover, it provides a description of the post processing step and SCR onsets detection analysis applied to real EDA data. The fifth Chapter shows the results obtained from both synthetically generated and experimentally acquired EDA data. Discussion of the results is presented in the sixth Chapter, while the last Chapter draws the conclusions and discusses the limitations of this work presenting some ideas about how to proceed in the future to further develop the work.

CHAPTER 1

STATE OF THE ART

1.1 ELECTRODERMAL ACTIVITY

ElectroDermal Activity (EDA), also known as Galvanic Skin Response (GSR) or Skin Conductance (SC), is a signal reflecting changes in the electrical properties of the skin resulting from the Autonomic Nervous System (ANS) activity [12]. These fluctuations are caused by activations of sweat glands which cannot be controlled consciously [11],[12]. Whenever sweat glands are triggered, moisture is secreted through pores towards the skin surface [11]. The balance of positive and negative ions in the secreted fluid is changed resulting in variations of skin conductance which can be recorded non-invasively using two electrodes placed on the skin [11].

EDA, controlled only by the sympathetic nervous system, can be considered to be a marker of both psychological and physiological arousal and, by extension, a measure of emotional and cognitive activity [12].

1.2 ANATOMICAL AND PHYSIOLOGICAL EDA SIGNAL BASIS

The skin is a selective barrier whose functions are to both prevent entry of foreign matter into the body and to selectively facilitate passage of materials from the bloodstream to the exterior of the body [13]. Moreover, by means of both vasoconstriction/dilation and variation in the production of sweat, it helps to maintain water balance and constant core body temperature [13]. Since the skin constantly receives signals from control centers in the brain, Edelberg pointed out that "we can listen in on such signals by taking advantage of the fact that their arrival at the skin is heralded by measurable electrical changes that we call electrodermal activity" [13].

Two types of sweat glands are present in the human body: the apocrine type, and the eccrine one. Although thermoregulation is the primary function of most eccrine sweat glands, all eccrine glands are believed to be involved in psychological sweating, with the ones located on the palmar and plantar surfaces suggested to be the most responsive to psychologically significant stimuli: psychological sweating is more evident in these areas probably because of the high gland density [13]. EDA measurement is mostly concerned with psychologically induced sweat gland activity [13].

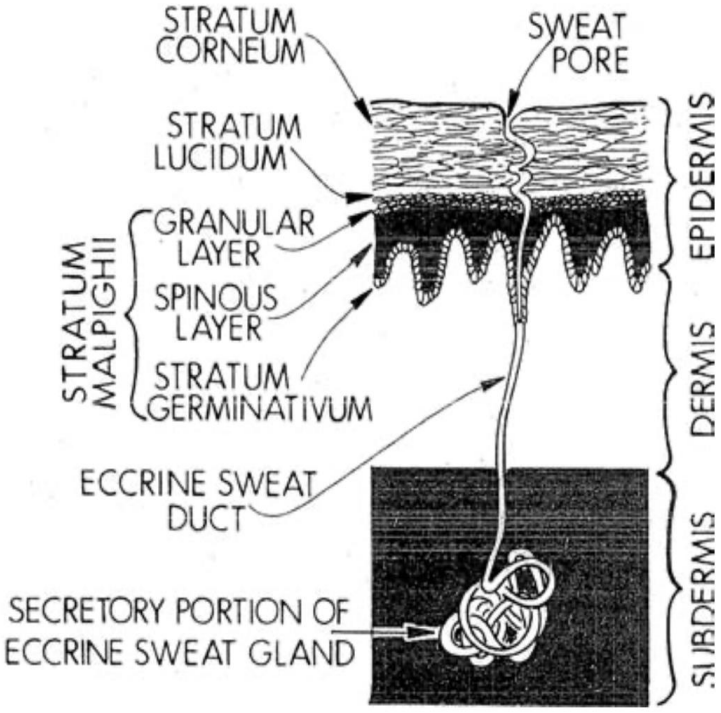

Figure 1. Eccrine sweat gland structure within the skin [13].

As shown in Figure 1, the skin is characterized by a layered composition. The stratum corneum is the extreme outer coat of the skin consisting of a layer of dead cells whose function is to protect the internal organs. Below it, the stratum lucidum and the stratum Malpighi lie. As regards an eccrine sweat gland, it consists of two portions: the secretory portion of the gland, characterized by a coiled compact body and the excretory portion of the gland, characterized by a sweat gland duct [13]. As shown in Figure 1, the sweat duct is relatively straight in its path through the stratum Malpighi and stratum lucidum, whereas it then spirals through the stratum corneum opening on the surface of the skin as a small pore [13].

By considering the sweat ducts, that are the tubular portion of the gland opening onto the skin surface, as a set of variable resistors wired in parallel, it is possible to relate EDA to sweat glands. Varying amounts of sweat, in varying numbers of sweat glands, will rise in the duct depending on the degree of activation of the sympathetic nervous system. The higher the sweat, the lower the resistance in that specific variable resistor, so that changes in the level of sweat in the ducts change resistors values providing observable changes in the EDA signal [13].

From an historical point of view, EDA was believed to be influenced by both the sympathetic and parasympathetic divisions of the ANS. Nowadays, it is agreed that human sweat glands have

predominantly sympathetic cholinergic innervation from sudomotor fibers originating in the sympathetic chain, so that EDA is controlled by the sympathetic division of the ANS [13]. Since there are a lot of brain parts responsible for influencing the sympathetic nervous system, the neural pathways underlying the central control of EDA are several and complex.

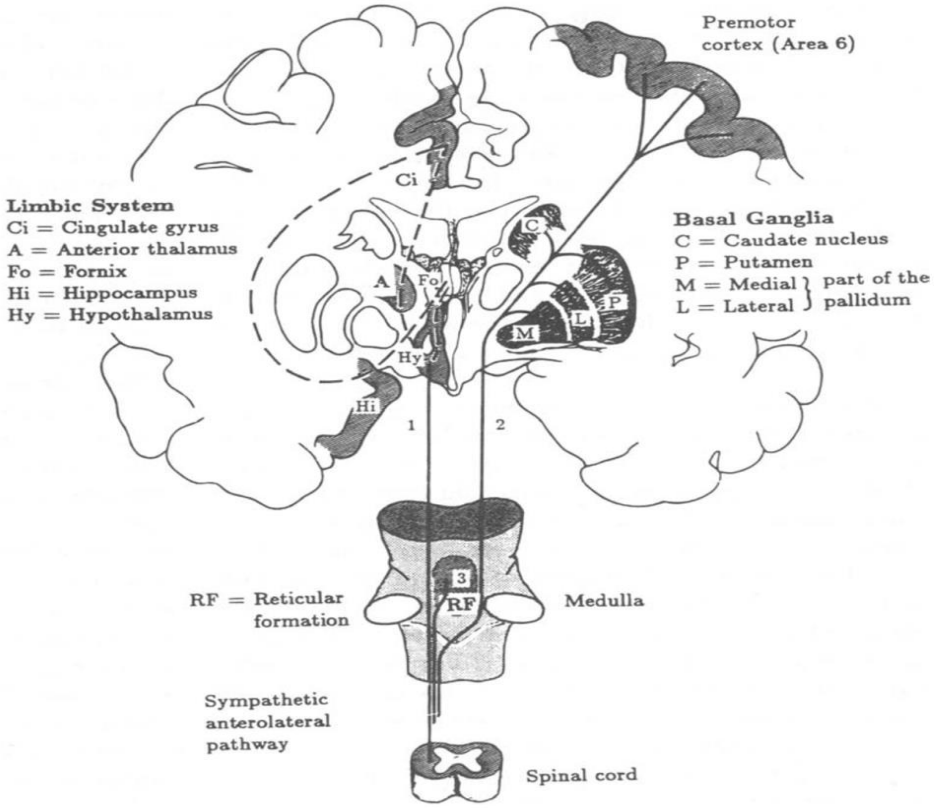

Figure 2. Central nervous system determinants of EDA in humans [13].

As shown in Figure 2, there are three relatively independent neural pathways involved in the EDA control. The first and most important one involves contralateral cortical and basal ganglion influences, the second level of EDA control involves ipsilateral hypothalamus and limbic system influences and the third one involves the reticular formation in the brainstem [13].

1.3 EDA SIGNAL ANALYSIS

1.3.1 EDA SIGNAL COMPONENTS AND METRICS

EDA signal can be analyzed both in the time and frequency domain.

In the time domain, the EDA signal consists of two main components: the tonic component or skin Conductance Level (SCL) and the phasic component or Skin Conductance Response (SCR).

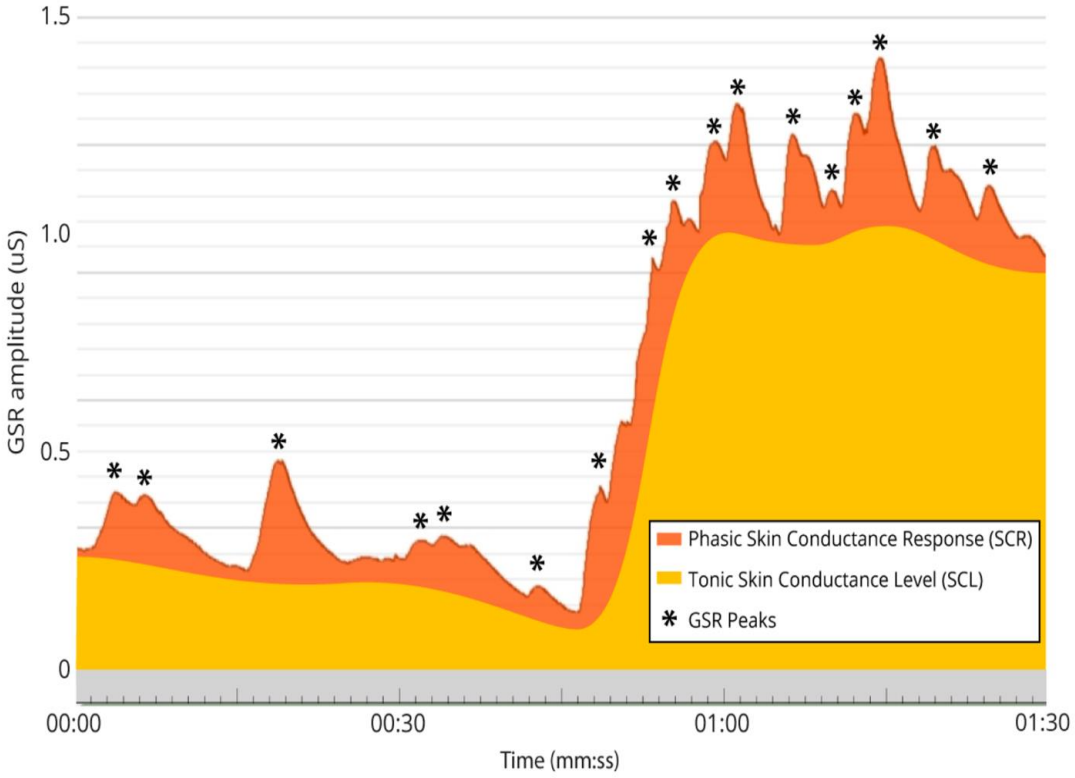

Figure 3. An example of time domain EDA signal representation and its components [11].

The tonic component, or SCL, is the low-frequency component of the EDA signal and slowly changes in time. Such component can vary markedly across subjects depending on their hydration, skin dryness and autonomic regulation. Due to these interpersonal differences, an SCL analysis on its own is not that informative [11].

The phasic component, or SCR is, instead, the high-frequency component of the EDA signal. It is characterized by fast variations called GSR or EDA peaks. SCR may be event-related SCR (ER-SCR), if

it is sensitive to specific emotionally arousing stimuli (sounds, images), or non-specific SCR (NS-SCR), if its occurrence is not a consequence of any eliciting stimulus [11].

Individual SCRs can be characterized by the following four metrics, as shown in Figure 4:

• Latency. It is defined as the time interval between the stimulus onset and the GSR peak onset. Typically, ER-SCRs arise 1-5 seconds after the stimulus. The peak onset is generally set to the time point where the GSR curve exceeds a minimum amplitude criterion (0.01 μS or 0.05 μS).

• Peak amplitude. It is defined as the amplitude difference between the onset and the maximum of the peak.

• Rise time. It is defined as the time interval between the onset and the maximum of the peak.

• Recovery time. It is defined as the time interval from peak to total recovery. Usually, the recovery time is quite longer than the rise time [11].

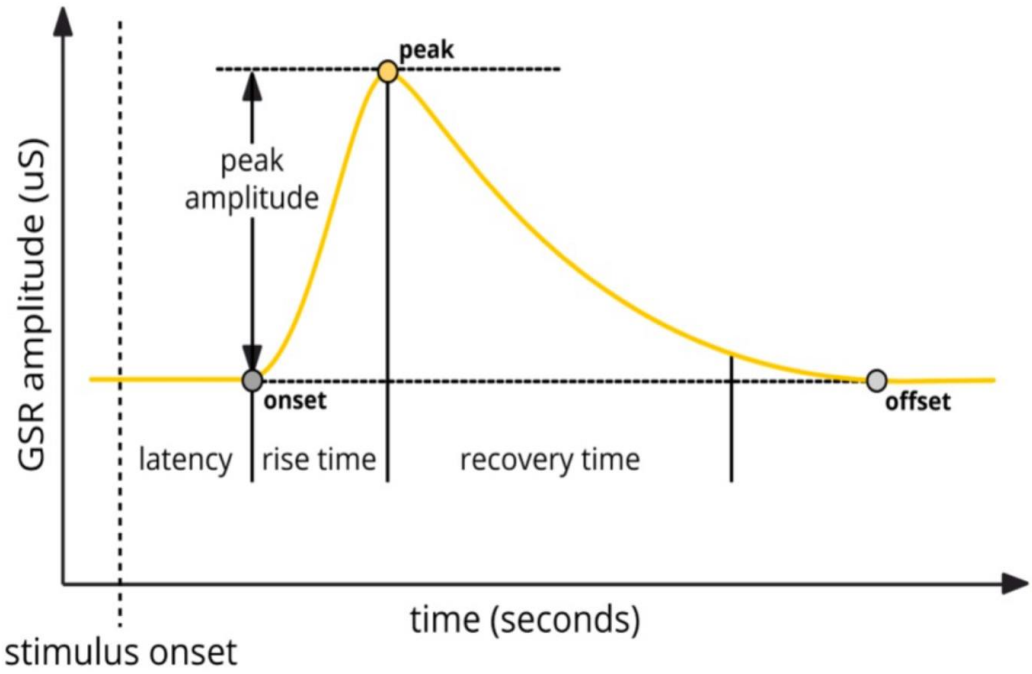

Figure 4. An individual SCR with its four metrics [11].

1.3.2 EDA SIGNAL ACQUISITION AND DEVICE PLACEMENT

There are three different methods to measure EDA signal: one without the application of an external current, which is called the endosomatic method, and two exosomatic methods, which either apply a direct current (DC) through electrodes to the skin, or an alternating current (AC) [14].

In the endosomatic method, an electrical potential difference can be measured across the palmar and plantar skin in the absence of any applied voltage or current. A single electrode is placed on the active site with a reference electrode at a relatively inactive site such as the forearm [14].

In the exosomatic method with DC, a constant small voltage (e.g., 0.5 V) is applied between the two electrodes placed on the skin surface. As result, applying Ohm's law, the skin resistance (SR) or its reciprocal, the skin conductance (SC), can be calculated [14].

In the exosomatic method with AC, there is the measurement of the skin impedance or of its reciprocal, defined as the skin admittance [14].

While sweat glands are present on almost all parts of the body, there are certain areas which respond more strongly to emotional stimulation. The most sensitive recording areas are at palmar sites, defined as medial and distal phalanges of middle and index finger, or thenar and hypothenar eminence areas and at the feet or wrist [11],[15].

EDA devices typically consist of two electrodes, an amplifier and a digitizer and, in the case of wireless devices, also data transmission modules for communication with the recording computer (using the Bluetooth protocol, for example) [11]. Some devices allow arbitrary sensor placements in any of the locations mentioned above, whereas other devices have electrodes rigidly mounted and integrated in wristbands or elastic straps [11].

1.4 EDA SIGNAL PROCESSING

The raw EDA signal has to be first pre-processed in order to remove noise and possible motion artefacts. Electrical noise is removed from the signal by applying a low-pass filter with a very small cut-off frequency (usually less than 1 Hz) whereas the most basic approach to remove motion artefacts is low pass filtering and manual inspection of the signal [15]. Once the EDA signal has been pre-processed, it can be decomposed in SCL and SCRs components since their individual analysis, and especially the analysis of SCRs, yields more significant information about emotional arousal of a subject [15].

The detection of peaks and troughs in a time series is what most traditional scoring SCRs algorithms count upon [6]. These algorithms look for the time-series points where the derivative of the signal is zero to determine the presence of a peak or trough, and then they measure the amplitude and rise-time of an SCR relative to its onset [6].

A shortcoming of these algorithms becomes evident in the presence of SCRs overlapping, a situation very common in experiments using short inter-stimulus intervals [6]. The problem in such situations is that, in the presence of SCRs overlapping, the tail of the preceding SCR yields a higher baseline for the following SCR which, in turn, causes the measured SCR amplitude to be smaller than the true amplitude, since it is measured relative to the higher baseline [6]. Moreover, the tail of the preceding SCR hides the initial effects of the next SCR which, in turn, causes the measured onset time to be delayed relative to the true onset time, and the measured rise-time to be less than true rise-time [6]. In a nutshell, the problem of overlapping SCRs yields distortions into all SCR measures. To face this problem, several mathematical models and decomposition methods have been developed to analyze the EDA signal more accurately.

Alexander et al. [6] proposed an automated analysis method based on the mathematical process of deconvolution [6],[7]. The hypothesis underlying this method is that sudomotor nerve activity shows sudomotor bursts, or peaks, with short time constants which, in turn, trigger SCRs having larger time constants [8]. This way, the EDA signal is the result of a convolution process between the sudomotor nerve signal (corresponding to a driver function) and an impulse response function [7]. By deconvolving the EDA signal with a specific impulse response function (IRF) (also called transfer function) the driver function, which is a sequence of discrete bursts, is revealed [7],[8]. The IRF depicts the SCR shape resulting from a unit impulse and it is a biexponential function, the so-called Bateman function, with the parameters $\tau_1 = 0.75\ s$ and $\tau_2 = 2$ with these 2 time constants representing the steep onset and slow recovery, respectively [7]. The physiological rationale underlying this biexponential function comes from a two-compartment diffusion process proposed by Schneider [7].

Since the resulting driver shows distinct impulses (the term impulse here means a peak or deflection in the driver function nonetheless showing a limited but significant duration), they can be extracted from the signal and used to reconstruct the corresponding SCRs. [6] shows that the scores coming from the reconstructed SCRs were similar to those obtained from the trough-to-peak method. To summarize, this decomposition method involves:

1. deconvolution of the EDA signal, to obtain the driver function;

2. isolating single impulses in the driver function;
3. convolution of the peaks identified in the driver function with a biexponential function, to reconstruct the individual SCRs [6].

There are some shortcomings associated to this method. The hypothesis on which deconvolution is based is that a standard SCR shape, or IRF, exists. Unfortunately, several studies point out not only a significant inter-individual variability in SCR shape but also a significant intra-individual variability [8]. [7] shows that deviations of the data from a model IRF may yield implausible driver responses. For slow recovery process of the IRF (high time constant τ_2), the driver may become negative for some SCRs which is something that cannot be interpreted in terms of sudomotor activity whereas, for fast recovery process of the IRF, less compact impulses in the driver function result from the deconvolution [6],[8].

To face this problem, Benedek and Kaernbach proposed an EDA signal decomposition method based on nonnegative deconvolution, called Discrete Decomposition Analysis (DDA) [7]. Unlike [6], this method claims nonnegativity of the driver and maximal compactness of the impulses [8]. With this decomposition method, it is possible to estimate both the tonic and phasic component. The tonic component can be estimated using a fit of the inter-impulse intervals of the driver resulting from standard deconvolution, and the phasic component can then be extracted from the EDA signal by subtracting the SCL from it [8]. By applying nonnegative deconvolution to the phasic component, two phasic signals, namely a nonnegative phasic driver and a remainder, emerged [8]. The phasic driver shows a zero-baseline intermitted by distinct peaks, whereas the remainder signal accounts for all deviations from the standard SCR shape [8]. Therefore, with this method, any negative component of the driver is transformed into a positive remainder, which can be interpreted as the additional phasic component resulting from additional sweat diffusion caused by pore opening as hypothesized in the poral valve model by Elderberg [8],[15].

DDA accounts for inter-individual differences in the SCR shape and selects the most adequate τ parameters for the IRF during an optimization procedure. Finally, the recompositing of all extracted components results in a valid reconstruction of the original EDA signal [8].

Benedek and Kaernbach, then, proposed another EDA signal decomposition method called Continuous Decomposition Analysis (CDA), always based on a standard deconvolution algorithm [8]. With CDA, the problem of the varying SCR shape was faced differently from [7] since the SCRs shape variation is not made attributable to the poral valve model of Edelberg [8]. The concept of single, discrete responses is left behind in favor of a continuous measure of phasic activity, considered to

be an adequate indicator of sympathetic activity and, by means of response window integration, an indicator of event-related activity is easily computed [8]. To summarize, this decomposition method involves the deconvolution of the EDA signal and the subsequent estimation of tonic and phasic activity [8].

The Ledalab toolbox, developed by Benedek and Kaernabach, implements both DDA and CDA decomposition methods [7],[8],[10].

CHAPTER 2

COMPRESSED SENSING

Traditionally, the exact recovery of a signal of interest can be obtained from a set of uniformly spaced samples taken at the Nyquist rate of twice the highest frequency present in the signal [17]. One problem is that in many emerging applications, the required Nyquist rate could be so high that it may be too expensive or physically impossible to build devices able of to acquire samples at that rate [16],[17].

Compressed Sensing or Sampling (CS) has emerged as a new sensing/sampling paradigm for signal acquisition and sensor design enabling a reduction in the sampling and computation costs for signals having a sparse or compressible representation. The main idea behind CS is to find ways to directly sense the data in a compressed form, thus at a lower sampling rate, rather than what usually is done, that is, first sampling at a high rate and then compressing the sampled data [16],[17].

CS involves three main processes: sparse representation, linear measurement and recovery [18].

2.1 SPARSE REPRESENTATION PROCESS

2.1.1 LOW-DIMENSIONAL SIGNAL MODELS

Let's start this section by saying that, in order to design efficient algorithms to acquire, process and extract information from a signal of interest, the first thing to do is to model the signal somehow. In general, signals have been modeled as vectors living in a certain vector space [17].

Here the focus is on low dimensional signal models and in particular on sparse models for finite dimensional signals. The rationale behind these types of structures is that the degrees of freedom of high dimensional signals are actually small compared to their ambient dimensionality [17].

2.1.2 SPARSE MODELS

As reported above, sparse signal models express the idea that little information is contained in high dimensional signals with respect to their ambient dimension [17].

Mathematically, a signal x can be modeled as k-sparse when it has at most k nonzero entries, i.e.

$$|x|_0 \leq k \qquad (1)$$

where $|\cdot|_0$ is the l_0 norm. k_x is also called sparsity level of the signal x.

$\Sigma_k = \{x: |x|_0 \leq k\}$ represents the set of all k-sparse signals [17].

Sometimes, signals can be considered themselves sparse; in other cases, they can have a sparse representation in some basis.

Having said that, few natural signals are exactly sparse. They are compressible or approximately sparse, instead. It is possible to quantify the compressibility of a signal by computing the error coming from approximating the signal, x, by some $\hat{x} \in \Sigma_k$:

$$\sigma_k(x)_p = min_{\hat{x}\in\Sigma_k}|x - \hat{x}|_p \qquad (2)$$

If $x \in \Sigma_k$,then $\sigma_k(x)_p = 0$ for any p [17].

Another way to express the compressibility of a signal is by saying that the sorted magnitudes of its coefficients decay quickly, or that most of the signal's energy is concentrated in only few entries [20]. Since the magnitudes of their coefficients decay rapidly, compressible signals can be represented accurately by $k \ll n$ coefficients [17].

In summary, either the signal is naturally sparse, or a sparse representation process is performed by projecting the original signal on a suitable basis where it can be modelled as sparse.

2.2 LINEAR MEASUREMENT PROCESS

Let's focus on the standard finite-dimensional CS model. The linear measurement process, or encoding, consists of multiplying the sparse signal with a sensing matrix. We have a signal $x \in R^n$ and a measurement system acquiring m linear measurements. Mathematically,

$$y = Ax \qquad (3)$$

where $y \in R^m$ is the measurements vector and A is a $m \times n$ sensing matrix with $m \ll n$, therefore representing a dimensionality reduction. The measurements are non-adaptive, meaning that the rows of A are fixed in advance and do not depend on the previously acquired measurements [17].

The aim of the sensing matrix A is to sample and compress, simultaneously, the original sparse signal below the Nyquist rate [18]. In this process, it is important to select or design a sensing matrix with specific properties in order to recover the original signal x from measurements vector y . Two

requirements need to be met by the sensing matrix, namely the restricted isometry property (RIP) and the coherence [18].

2.2.1 RESTRICTED ISOMETRY PROPERTY

When the measurements are affected by noise, in order to study the general robustness of CS, it is possible to resort to the Restricted Isometry Property (RIP) [16]. RIP characterizes orthonormal matrices which are bounded with a constant called restricted isometry constant ∂ [18].
A matrix A satisfies the RIP of order k if there exists a $\partial_k \in (0,1)$ so that
$(1-\partial_k)|x|_2^2 \leq |Ax|_2^2 \leq (1-\partial_k)|x|_2^2$ holds for all $x \in \Sigma_k$ [16],[19].
If a matrix A satisfies the RIP of order $2k$, it means that A approximately preserves the distance between any pair of k-sparse vectors [17]. Equivalently, it is possible to say that if A satisfies the RIP of order k, it means that all subsets of k columns of A are nearly orthogonal [16].
The RIP condition must be considered when designing the sensing matrix because if a matrix A satisfies the RIP, then this is sufficient condition for a variety of algorithms to be able to successfully recover a sparse signal from noisy measurements [17].

2.2.1.1 MEASUREMENT BOUNDS

How many measurements m are necessary to achieve the RIP? The following theorem answer this question: given the $m \; x \; n$ matrix A satisfying the RIP of order $2k$ with constant $\partial_{2k} \in (0,0.5]$, then $m \geq Cklog(\frac{n}{k})$ where $C \approx 0.28$ [17],[18].

2.2.2 COHERENCE

From a theoretical point of view, the RIP condition provides guarantees for the recovery of k-sparse signals. Nonetheless, the problem, in practice, with this condition is that to verify that a general matrix A satisfies this property would require a combinatorial search over all $\binom{n}{k}$ submatrices [17]. Therefore, more easily computable properties of A are used in order to provide recovery guarantees. One of these properties is the coherence of a matrix A , $\mu(A)$, which is defined as the largest absolute inner product between any two columns a_i, a_j of A:

$$\mu(A) = max_{1\leq i,j\leq n} \frac{|a_i^T a_j|}{|a_i|_2 |a_j|_2} \quad (4)$$

The following condition on A guarantees the uniqueness of the recovered solution:

If

$$k < \frac{1}{2}(1 + \frac{1}{\mu(A)}) \quad (5)$$

then for each measurement vector $y \in R^m$there exists at most one signal $x \in \Sigma_k$ such that $y = Ax$, where k is the level of sparsity [17],[18]

The importance of the coherence property derives from the fact that, the smaller the coherence, the fewer measurements are needed to reconstruct the original signal [16],[17].

2.3 SPARSE RECOVERY PROCESS

2.3.1 SIGNAL RECOVERY VIA l_1 MINIMIZATION

The recovery of the vector x from the observations y, with A being an over-complete matrix corresponds to solving an undetermined system of linear equations which is ill-posed [20].

The original sparse or compressible signal can be recovered from the measurements y by solving an optimization problem:

$$\hat{x} = arg\ min_z |z|_0 \ subject\ to\ z \in B(y) \quad (6)$$

It means that the sparsest x, consistent with the measurements y, is searched and found.

If the measurements are noise-free, then $B(y) = \{z: Az = y\}$.

If there is some noise in the measurements, then $B(y) = \{z: |Az - y|_2 \leq \varepsilon\}$ where ε bounds the noise in the data [16],[17].

Since the objective function $|.|_0$ is not convex, finding a solution of this problem is NP-hard: what can be done is to replace $|.|_0$ with $|.|_1$ thus operating a convex relaxation of the problem:

$$\hat{x} = arg\ min_z |z|_1 \ subject\ to\ z \in B(y) \quad (7)$$

This convex optimization problem can be solved by recovery algorithms, also called reconstruction algorithms. Recovery or reconstruction algorithms can be divided into 3 main categories: convex relaxation algorithms, Greedy algorithms and Bayesian-based recovery [18].

The idea behind all these algorithms is that, by requiring the matrix A to satisfy additional conditions, the problem of finding the unique sparse solution can be solved efficiently [19].
Convex relaxation algorithms work by solving the equation (6) by means of linear programming [19]. Examples are: Basis pursuit (BP), used if the measurements are noise-free, or Basis Pursuit denoising (BPDN), if there is some noise in the measurements.

2.3.1.1 NOISE FREE SIGNAL RECOVERY

For noise-free signal recovery, the following theorem holds. Given measurements of the form $y = Ax$, with $B(y) = \{z: Az = y\}$, if A satisfies the RIP of order $2k$ with $\partial_{2k} < \sqrt{2} - 1$, then the solution $\hat{x}$ to (2) obeys $|\hat{x} - x|_2 \leq C_0 \frac{\sigma_k(x)_1}{\sqrt{k}}$ [16],[17].

Therefore, provided that the matrix A satisfies the RIP, meaning $O\left(klog\frac{n}{k}\right)$ measurements are needed, it is possible to recover any k-sparse signal x exactly [16],[17],[18].

2.3.1.2 ROBUST SIGNAL RECOVERY FROM NOISY DATA

In case of uniformly bounded noise, the following theorem holds [16],[17].
Given $y = Ax + e$ where $|e|_2 \leq \varepsilon$ and $B(y) = \{z: |Az - y|_2 < \varepsilon\}$, if A satisfies the RIP of order $2k$ with $\partial_{2k} < \sqrt{2} - 1$, then the solution $\hat{x}$ to (2) obeys $|\hat{x} - x|_2 \leq C_0 \frac{\sigma_k(x)_1}{\sqrt{k}} + C_2\varepsilon$
From the theorem it is possible to see that the reconstruction error is bounded by the sum of two terms: the first term is the error in case of noise-free data, the second term is just proportional to the noise level [16],[20].

2.4 STABLE SEPARATION OF APPROXIMATELY SPARSE SIGNALS

We then shift our attention to the following recovery problem of the vector $x \in C^{N_a}$ from the corrupted M-dimensional observations:

$$z = Ax + Be + n \qquad (8)$$

where: $A \epsilon C^{M \times N_a}$ and $B \in C^{M \times N_b}$ are general deterministic dictionaries meaning bases, frames, or overcomplete matrices whose columns have unit l_2 norm [20].

This framework is very important in signal separation because it can also be used to model the decomposition, or separation, of signals into two distinct features Ax and Be from the noisy observation z, thus in a part that shows an approximately sparse representation in the dictionary A and another one that shows an approximately sparse representation in B [20]. An application of this framework is the decomposition of EDA signal in its 2 components as reported in [1]. In the signal separation or decomposition case, the vector e is assumed to be approximately sparse, as much as x, and is used to represent a second desirable feature [20].

The aim of signal separation is to simultaneously recover, or extract, the vectors x and e from the noisy measurement z and then compute the individual signal features Ax and Be [20].

In general, the recovery guarantees for such problem depend on: the number of dominant non-zero entries of x and e, the coherence parameters of the dictionaries A and B, the l_2-norm of the noise vector and also on the amount of knowledge on the location of the dominant entries available prior to recovery [20]. In the remainder of this section, the case where no knowledge on the support-set of the approximately sparse vector x and e is available is reported.

In this case, the idea is to rewrite (8) as:

$$z = Cw + n \tag{9}$$

Where: $C = [A\ B\ ]$ is the concatenated dictionary of A and B and $w^T = [x^T\ e^T\ ]$.

Once written this way, the signal separation or decomposition approach traces back to perform BPDN on (9) to recover w from z. A way to find recovery guarantees for this problem is to use theorem from the 'robust signal recovery from noisy data' section rewriting the recovery condition (5) as:

$$k_w < 0.5(1 + \frac{1}{\mu_c}) \tag{10}$$

Where: $k_w = k_x + k_e$ is the sparsity level of vector w and μ_c is the coherence of C defined as:

$$\mu_c = max_{i \neq j} \frac{|d_i^T d_j|}{|d_i|_2 |d_j|_2} = max\{\mu_a, \mu_b, \mu_m\} \tag{11}$$

The problem with this recovery guarantees approach is that it does not consider the underlying structure of C which is the concatenation of 2 dictionaries [20].

The following theorem solves this problem and refines the preceding condition.

Theorem 1. Given $z = Cw + n$ with $C = [A\ B\ ]$, $w^T = [x^T\ e^T\ ]$ and $|n|_2 \leq \varepsilon$, C is characterized by the coherence parameters μ_a , μ_b, μ_m, μ_C and $\mu_b \leq \mu_a$ is assumed.

If

$$k_w = k_x + k_e < max\{\frac{2(1+\mu_a)}{\mu_a+2\mu_c+\sqrt{\mu_a^2+\mu_m^2}}, \frac{1+\mu_c}{2\mu_c}\} \qquad (12)$$

then the solution $\widehat{w}$ to the problem:

$min\ ||\widehat{w}||_1\ \ subject\ to\ \ ||z - C\widehat{w}||_2 \leq \eta$, using $\eta < \varepsilon$, satisfies:

$$|\widehat{w} - w|_2 \leq C_1(\frac{\sigma_{k_w}(w)_1}{\sqrt{k_w}}) + C_2(\varepsilon + \eta) \qquad (13)$$

This theorem, properly modified, is used by [1] to obtain recovery guarantees for his compressed sensing decomposition approach of EDA signal as reported in the next chapter.

CHAPTER 3

MATERIALS AND METHODS

3.1 EMPATICA E4 WRISTBAND

The Empatica E4, shown in Figure 5, is a wearable wireless multi-sensor device for real-time computerized biofeedback and data acquisition [4]. The E4 wristband has four embedded sensors:

- photoplethysmography (PPG) sensor,
- electrodermal activity (EDA) sensor,
- 3-axis accelerometer,
- temperature sensor.

The EDA sensor is equipped with a peripheral board for EDA circuitry that, when worn, is placed on the ventral area of the wrist. The terminal part of the EDA sensor is composed of two silver-coated (Ag) hypoallergenic and durable electrodes, through which a small alternating current is applied to the skin. The EDA sensor can measure conductance in the $[0.01, 100]\ \mu S$ range with a default sampling rate of $4\ Hz$. The digital resolution is 1 digit per $900\ pS$ [4].

E4 wristband may work in two distinct modalities: real-time streaming and in-memory recording. With in-memory recording mode, data are stored into the internal flash memory and once the data are acquired, the device has to be connected via USB to a computer in order to import data to a cloud platform, named E4 Connect. This operation is performed automatically by a desktop application, the E4 Manager. In real-time streaming mode, the E4 wristband connects to smartphones or tablets via Bluetooth. A mobile application, *E4 Realtime*, allows the real-time visualization of data being acquired on the smartphone. When the acquisition ends, raw data is automatically uploaded to E4 Connect [4].

Raw data can then be downloaded in CSV format. In this thesis, only the “EDA.csv” file was downloaded and processed.

Figure 5. The Empatica E4 wristband [21].

3.2 THE PHYSIOLOGICAL RATIONALE UNDERLYING THE MODEL

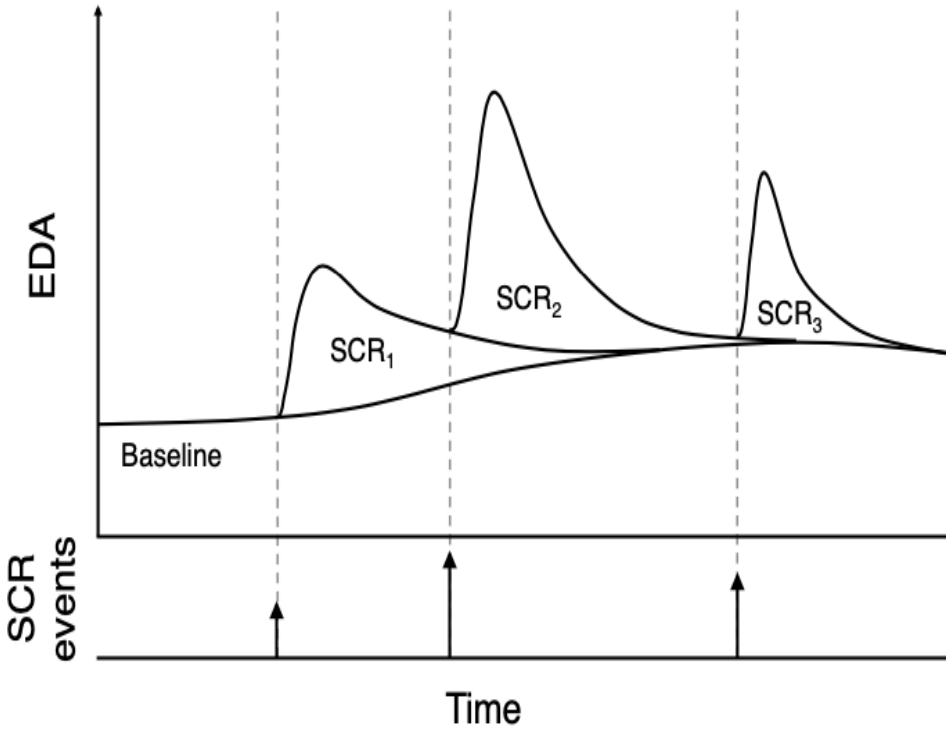

Figure 6. An EDA signal where SCR events are decomposed [5].

As shown in Figure 6, two components characterize the observed EDA signal. One is a slowly varying skin conductance level, the other consists of multiple short-lived, often overlapping, spike-like events, the SCRs, each arising from a corresponding SCR event [1].

A subject responds to a stimulus with the occurrence of a sparse selection of events, denoted SCR events, which drives the SCRs [1]. The SCR events signal can be seen as a train of impulses which correlates with sudomotor neuron bursts [1]. The sudomotor neuron bursts result in eccrine glands to expel sweat which, in turn, causes changes in skin conductance in the form of an SCR [1]. Expelling, pooling, and evaporation of sweat on the surface of the user's skin result into a specific SCRs' shape [1].

Moreover, some sweat is absorbed by the surface of the user's skin, which affects the SCL instead [1]. Last but not least, artefacts should be addressed: changes in the position of the sensors or in the amount of contact of the sensors with the skin, especially for wearable sensors, cause sudden shifts in the skin conductance denoted by jump discontinuities in the EDA signal [1].

3.3 DEFINITION OF THE MODEL

The observed EDA signal, y, is discretized into T time steps with the possibility of an SCR event at each time step [1]. Thus, the SCR events signal is denoted by a vector $x \in R^T$. After an SCR event, a sweat response or IRF (Alexander, Benedek) follows and this latter is denoted by a vector $h \in R^t$. The resulting SCR signal is therefore modeled as a linear time invariant (LTI) system where the SCR events signal x is convolved with the sweat response h, that is: $h * x \in R^{t*T-1}$.

Moreover, the SCR signal $h * x$ is superimposed on a baseline signal, denoted by a vector $b \in R^{t*T-1}$, consisting of SCL and motion artifacts. Finally, the observation noise is denoted by a vector $n \in R^{t*T-1}$. As shown in the Figure 6, the observed EDA signal y can then be represented as:

$$y = h * x + b + n \qquad (14)$$

In this model, the impulse response h is assumed to be known a priori whereas the SCR events signal x, the baseline b, and noise n to be all unknown [1].

A definition of the model components and a schematic of the implemented model are shown in Table 1 and Figure 7, respectively.

Table 1. Summary of the components of the model, along with their notation and description [1].

Components and notation	Description
SCR events, x	Skin conductance response event: an approximately sparse driver
Sweat response, h	Sweat response: impulse response function (IRF)
SCR, $h * x$	Skin conductance response: result of the convolution between x and h
Baseline, b	Baseline: SCL and motion artefacts
Noise, n	Noise: additive measurement noise

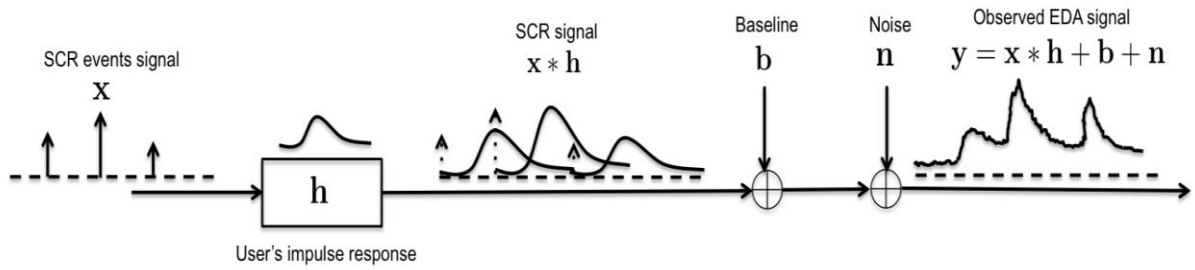

Figure 7. A schematic of the model and its components [1].

3.3.1 SCR EVENTS SIGNAL MODEL

A sparsity hypothesis on the SCR events signal is made. Specifically, the hypothesis is that a person cannot respond significantly to more than $s < T$ events. Such hypothesis formally means that the SCR events signal is assumed to lie in the set:

$$X_\delta^s = \{x | x \in R^T, \left|\left|x - x_s\right|\right|_1 \leq \delta\} \qquad (15)$$

Where: δ is a small constant and $x_s \in R^T$ has the s-largest magnitude, non-zero components of x. The formulation means that the above set is the collection of vectors which can be approximated within some distance δ ,in terms of the l_1 norm, from an exactly s-sparse signal [1].

3.3.2 BASELINE MODEL

Both baseline shifts, due to changes in the positions of sensors, and the SCL component are incorporated into the baseline signal b which is hypothesized to have jump discontinuities at no more than $c < t + T - 1$ locations. Such hypothesis formally means that the baseline signal is assumed to lie in the set:

$$B_\gamma^c = \{b | b \in R^{t+T-1}, \left|\left|Db - Db_c\right|\right|_1 \leq \gamma\} \tag{16}$$

Where: γ is a small constant, $D \in R^{(t+T-2)\times(t+T-1)}$ denotes the pairwise difference matrix defined as:

$$D = \begin{bmatrix} 1 & -1 & 0 & \cdots & 0 \\ 0 & 1 & -1 & \ldots & 0 \\ \vdots & \vdots & \ddots & \ddots & \vdots \\ 0 & 0 & \ldots & 1 & -1 \end{bmatrix} \tag{17}$$

and $Db_c \in R^{t+T-2}$ has the c-largest magnitude, non-zero components of Db. The formulation means that the above set is the collection of vectors which, after pairwise differencing, can be approximated within some distance γ, in terms of the l_1 norm, from a c-sparse signal [1].

3.3.3 NOISE MODEL

The observation noise n is hypothesized to be bounded by a fixed value ε, that is $||\frac{n}{2}||_2 \leq \frac{\varepsilon}{2}$ where $\varepsilon > 0$ [1].

As already stressed, the idea is to obtain the SCR events signal x from the EDA observation signal y given the prior information that $x \in X_\delta^s$ and $b \in B_\gamma^c$.

3.4 EDA SIGNAL DECOMPOSITION

Let's start by saying that due to the presence of the baseline b, the recovery of the true SCR events x from the observed EDA signal y is not easy. If no baseline but only noise had been present, the problem would have been that of a standard deconvolution in noise. By exploiting the added structure of the sparsity of the SCR events signal x , the latter could have been estimated with provable guarantees, as shown in [1].

The idea here, instead, is to exploit the structure of the baseline signal to help recovering x. Specifically, by assuming that the baseline signal has almost the same consecutive components for most of the signal elements, it can be converted to an approximately sparse signal by multiplying it with the above mentioned pairwise difference matrix D [1].

The process, as depicted in Figure 8, is the following:

- the observation signal y is linearly transformed using D(pre-processing step):

$$Dy = DT_h x + Db + Dn \tag{18}$$

Where: $T_h \in R^{(t+T-1)\times T}$ is a Toeplitz matrix, built from $h \in R^t$, and defined as:

$$T_h = \begin{bmatrix} h_1 & 0 & \dots & 0 \\ h_2 & h_1 & \vdots & \vdots \\ \vdots & \vdots & \ddots & 0 \\ h_t & h_{t-1} & \vdots & h_1 \\ 0 & h_t & & \\ \vdots & \vdots & \ddots & \\ 0 & \dots & \dots & h_t \end{bmatrix} \tag{19}$$

This way, the transformed baseline signal Db is approximately sparse, as much as the SCR events signal x , because of the structure of $b \in B_\gamma^c$ [1].

The terms are rearranged so that the model can be written as:

$$Dy = [DT_h \quad I] \begin{bmatrix} x \\ Db \end{bmatrix} + Dn \tag{20}$$

where: I is the identity matrix, $C = [DT_h \quad I]$ is our sensing matrix having less rows than columns and $w = \begin{bmatrix} x \\ Db \end{bmatrix}$ is the approximately sparse vector with $s + c$ significant , non-zero components to be estimated. This recovery problem setting is the same as the one described by equation (9) of Chapter 2.

- Finally, x and Db are jointly estimated by solving the following convex optimization problem using recent findings in compressed sensing field (6) as outlined in Chapter 2 of this thesis:

$$min\ ||\hat{x}||_1 + ||\hat{u}||_1\ \ subject\ to\ \ ||Dy - [DT_h\ \ I]\begin{bmatrix}\hat{x}\\ \hat{u}\end{bmatrix}||_2 \leq \eta \qquad (21)$$

where: $\hat{u}$ stands for Db and $\eta > 0$ is an optimization parameter whose value depends on the energy of noise n.

Theorem 1, from Chapter 2 of this thesis, ensures recovery guarantees for this particular compressed-sensing decomposition framework [20].

The above model and problem have been implemented in Matlab and solved using CVX software [9].

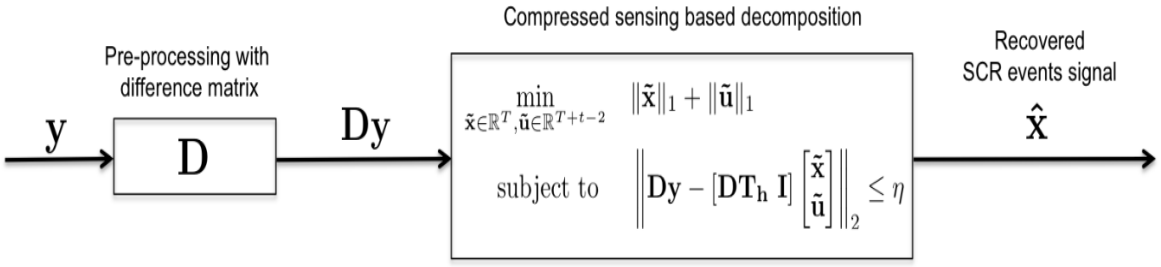

Figure 8. A schematic of SCR events signal recovery using compressed sensing-based decomposition [1].

3.5 EXPERIMENTAL PROTOCOL

Each EDA signal acquisition lasts about 12 minute and is composed by:

- the first 5 minutes of acquisition at resting condition where no sound is presented to the subject,
- the central 2 minutes of acquisition where 3 unpleasant sound stimuli are presented to the subject,
- the last 5 minutes of acquisition where no sound is presented to the subject.

The 3 isolated unpleasant sound stimuli, each lasting 6 seconds, are taken from the International Affective Digitized Sounds (IADS-2) database. This database contains a collection of sounds rated in terms of valence, arousal and dominance using Self-Assessment Manikin (SAM) scale [22].

The description and overall scores of the 3 sounds selected for the experiment are presented in Table 2.

For each of 6 EDA signals recorded, the 3 isolated unpleasant sound stimuli are played at 5:30 mm:ss(minutes:seconds), 6:30 mm:ss, and 7:00 mm:ss into the acquisition, respectively.

Table 2. Valence, arousal and dominance scores (dimensionless values) of the selected sounds in a mixed population.

Sound Description	Valence	Arousal	Dominance
Scream	2.05 ± 1.62	8.16 ± 2.15	2.55 ± 2.01
Car wreck	2.04 ± 1.52	7.99 ± 1.66	2.29 ± 1.74
Buzzer	2.42 ± 1.62	7.98 ± 1.99	2.84 ± 2.11

CHAPTER 4

EXPERIMENTS

4.1 SYNTHETIC EDA DATA EXPERIMENT

To test the feasibility and accuracy of the compressed sensing-based decomposition, both synthetic and real-world EDA data are used.

In particular, the aim of synthetic EDA data experiment is to evaluate the recovery accuracy of such a framework.

The procedure carried out is the following one:

- the impulse response vector h was obtained by sampling the biexponential function $f(u) = 2(e^{\frac{-u}{\tau_1}} - e^{\frac{-u}{\tau_2}})$ with $\tau_1 = 10$ and $\tau_2 = 1$, at the rate of 4 samples per second in the interval $u \in [0,40]$ as shown in Figure 9.
- $T = 240, \delta = 0.01, \gamma = 0.01$
- approximately sparse vectors $x \in X_\delta^s$ and $b \in B_\gamma^c$ are randomly generated with a certain number of SCR events s and baseline jumps entries c , respectively.
- specifically, a random x is produced by:

    1. picking the s significant components uniformly at random
    2. stuffing these components with a random vector with independent and identically exponentially distributed entries
    3. adding to it a rescaled standard Gaussian random with l_1 norm δ

- specifically, a random Db is produced by:

    1. picking the c significant components uniformly at random
    2. stuffing these components with a standard Gaussian variable
    3. Adding to it a rescaled standard Gaussian random vector with l_1 norm γ

- the noise n is a rescaled Gaussian random vector with l_2 norm equal to $\varepsilon = 0.01$
- the following observations are produced:

$$Dy = DT_h x + \alpha Db + n \qquad (22)$$

Several observations, using varying values of α ($\alpha = 0.01, \alpha = 0.1, \alpha = 1$), a scaling factor applied to Db relative to $DT_h x$, are carried out and employed to find the reconstructed $\hat{x}$ by solving the convex optimization problem (21) with an optimization parameter $\eta = 1.05\ \varepsilon$.

The metric used to evaluate the recovery accuracy of this framework is the recovery error R, also called reconstruction error, defined as the norm of the difference between the original signal x and the recovered signal $\hat{x}$, divided by the original signal's norm [18]. Thus, it can be written as:

$$R = \frac{\| x - \hat{x} \|_2}{\| x \|_2} \qquad (23)$$

Using the average recovery error from 5 random observations for several values of s and c ,recovery error diagrams are built and shown in the Results Chapter.

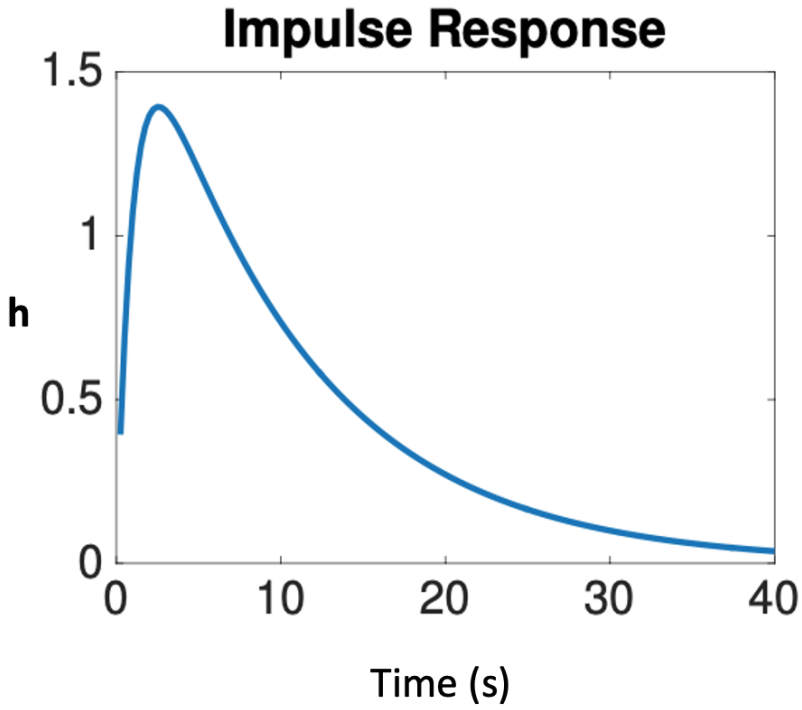

Figure 9. The impulse response obtained by sampling the function $f(u)$ [1].

4.2 EDA SIGNAL ACQUISITION

The EDA signal of 6 subjects (3 males and 3 females, aged between 20 and 60 years old) was recorded during an audio stimuli experiment using Empatica E4 wristband with a sampling frequency of 4 Hz.

4.3 THE POST-PROCESSING STEP

The goal of the post-processing step is to build a physiologically meaningful spike train, or activation sequence, of SCR events, as sparse as possible.

A problem with the reconstruction algorithm is that, in order to decrease the mean square error, it includes some impulses which are unphysiological and interfere with the interpretability of the recovered SCR events $\hat{x}$. Thus, the recovered SCR events signal needs to be processed.

Due to the existence of a refractory period, a hypothesis on non-overlapping SCR events is made.

The following algorithm, starting from the previously mentioned considerations, tries to take into account this situation:

- First, it sorts the elements of the recovered SCR events signal $\hat{x}$ in descending order according to their norm.
- Then, for $i = 1$:length($\hat{x}$), if the location of the i-th impulse $\hat{x}(i)$ is not within φ seconds of an existing impulse, the i-th impulse is added to the set of accepted impulses. Else, it is rejected.
- Finally, it rejects the accepted impulses whose norm lies below a certain threshold ψ sized on the max impulse found.

4.4 SCR ONSETS DETECTION ANALYSIS

In order to perform SCR onsets detection analysis, the 6 EDA traces acquired are divided into time windows of $10s$ (40 samples).

Then, the number of SCR onsets, whose locations correspond to the positions of the non-zero elements of the SCR events signal after the post-processing step, is computed in each time window and a vector, called Compressed-sensing (CS) SCR onsets vector, is created. The length of this vector

is equal to the number of time windows which the SCR events signal is divided into and its *i-th* element contains the number of detected SCR onsets in the *i-th* time window.

The Ledalab standard trough-to-peak (TTP) analysis [10] is then applied to each EDA signal acquired and a vector similar to the previously described one is created and named Ledalab (LL) SCR onsets vector. Its elements represent the number of SCR onsets detected by LL in each time window. The "Pocket guide" algorithm [11] is finally applied to each EDA signal acquired, and a vector similar to the previously described one is created and called Pocket guide (PG) SCR onsets vector. Its elements represent the number of SCR onsets detected by the PG-based method in each time window. Both the LL and PG SCR onsets vectors share the same length with the CS one.

The element-wise differences between the LL SCR onsets vector and the CS SCR onsets vector, and between the PG SCR onsets vector and the CS SCR vector are then computed and two difference vectors are created as a result. They are called delta (Δ) LL-CS vector and delta (Δ) PG-CS vector, respectively. Therefore, the LL and PG SCR onsets vectors act as control groups against which the SCR onsets detection ability of the proposed CS-based decomposition approach is tested.

A score (either 1 or 0) is given to each Δ vector element according to the following algorithm:

for i=1 to length (Δ)

if $\Delta(i)$ is equal to zero, then score(i):=1

else, score(i):=0

The sum of all elements of this new binary vector, named score, is computed to obtain a global score (GS) which is then expressed as a percentage as shown in the Results chapter.

As a result, each Δ vector, either LL-CS or PG-CS, is associated to a global score, expressed as a percentage which reflects the number of time windows where both LL and CS approaches or PG and CS approaches detect the same number of SCR onsets. Therefore, GS can be interpreted as a measure of the accuracy of the CS-based approach in detecting SCR onsets compared to Ledalab approach or Pocket guide approach, respectively.

Moreover, the mean and standard deviation of Δ vectors are computed and shown in the Results Chapter.

Finally, Figure 10 shows a schematic that sums up the approach described in this Chapter.

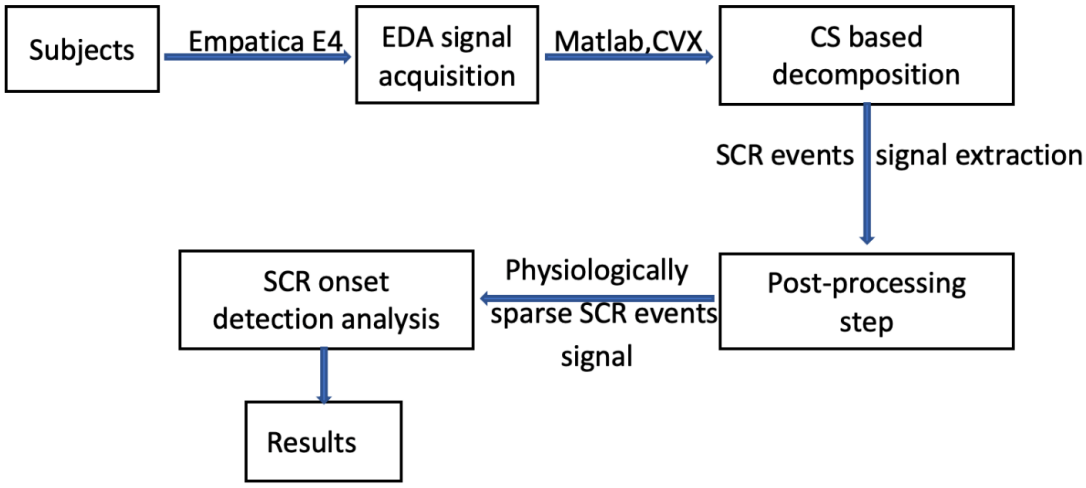

Figure 10. A schematic of the approach described in this Chapter.

CHAPTER 5

RESULTS

5.1 SYNTHETIC EDA DATA

In Figure 11, 3 synthetic data recovery error diagrams (a, b, c), one for each value of the coefficient α ($\alpha = 0.01,\ \alpha = 0.1,\ \alpha = 1$) are shown. In each diagram, the average recovery error value, for each possible combination of SCR events s varying in the discrete set $s \in \{10,20, \dots 240\}$ and of baseline jumps c varying in the discrete set $c \in \{10,20, \dots 350\}$, are computed and reported as a colored pixel.

Each Panel (a, b, c) shows a recovery error diagram with a different scaling parameter α ($\alpha = 0.01,\ \alpha = 0.1,\ \alpha = 1$) which scales the energy of the baseline component relative to the SCR component.

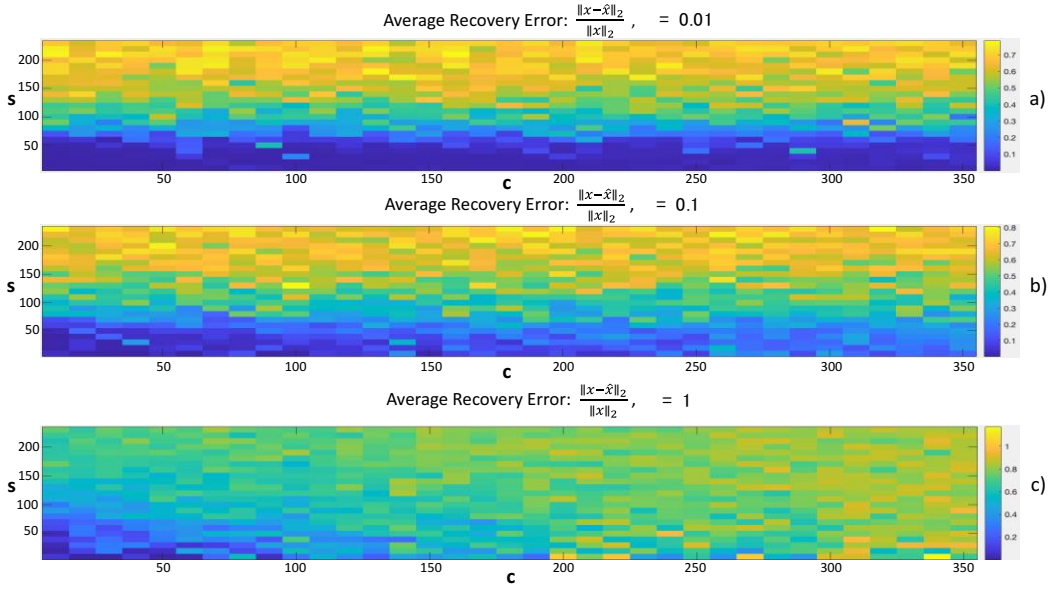

Figure 11. The synthetic data recovery error diagrams for a number of SCR events s varying in the discrete set $s \in \{10,20, \dots 240\}$ and for a number of baseline jumps c varying in the discrete set $c \in \{10,20, \dots 350\}$. The average recovery error, computed for each combination of s and c , is expressed as a pixel and a colorbar is added to each diagram to show the current colormap. Each Panel (a, b, c) corresponds to different scaling parameter α ($\alpha = 0.01,\ \alpha = 0.1,\ \alpha = 1$) which scales the amplitude of the baseline component relative to the amplitude of the SCR component.

5.2 REAL EDA DATA

In Figure 12, the 6 EDA traces acquired using Empatica E4 wristband along with the time location of the 3 audio stimuli, are shown.

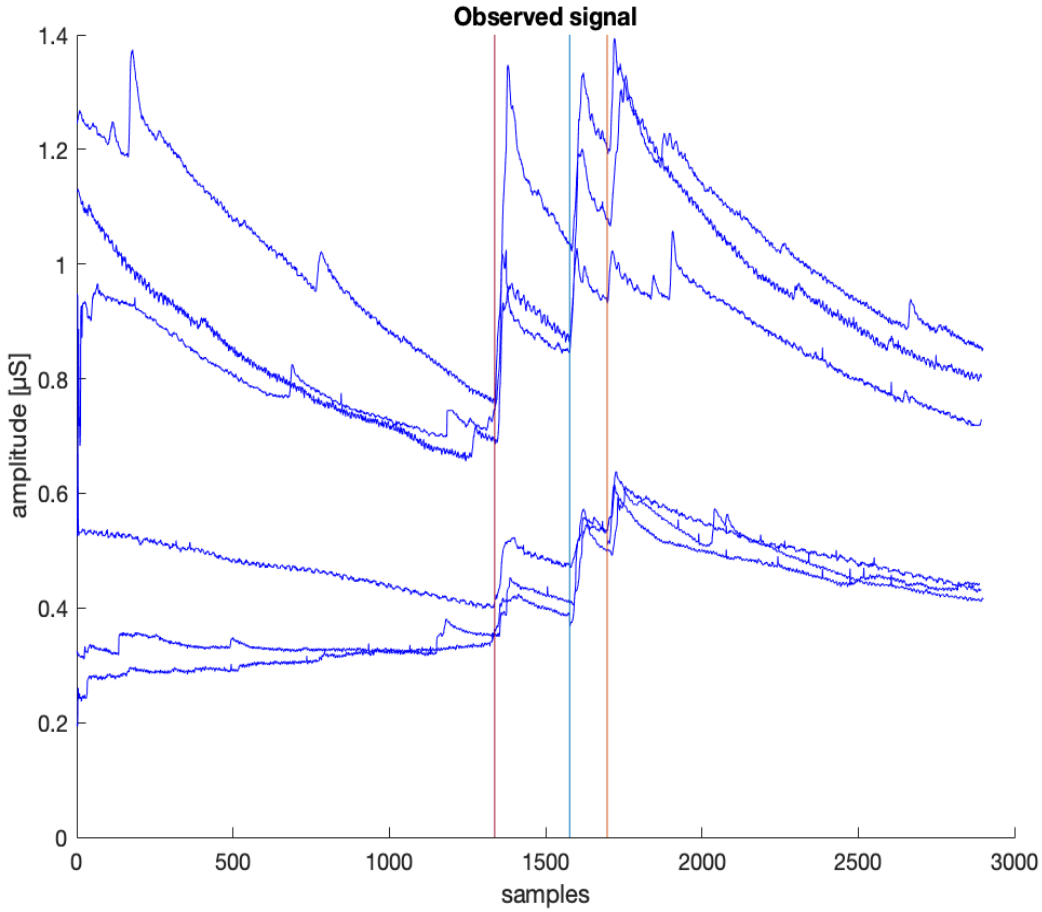

Figure 12. The 6 EDA traces acquired using Empatica E4, along with the 3 audio stimuli.

5.2.1 EDA SIGNAL DECOMPOSITION RESULTS

In Figures 13-18, for each of the 6 subjects, the signals obtained at each step of the proposed compressed sensing-based decomposition framework are reported. In each figure: panel a) shows the observed EDA signal y , panel b) shows the EDA signal y after the difference matrix D is applied (pre-processing step), the extracted SCR events signal $\hat{x}$ after the post-processing step are shown in panel c), and the reconstructed SCR component (phasic component of the EDA signal) computed as $h * x$, is shown in the panel d).

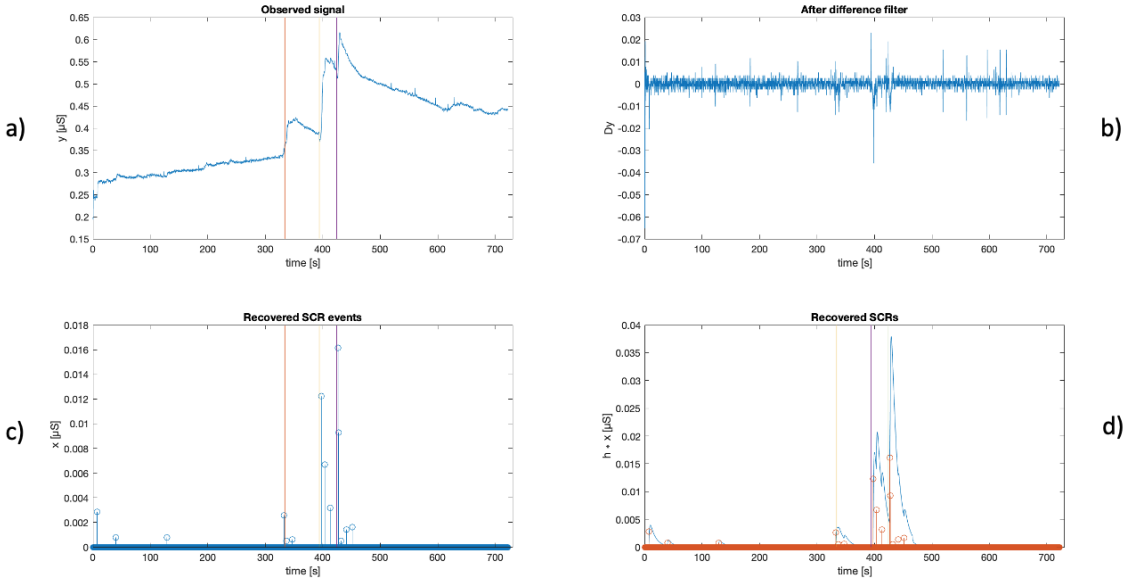

Figure 13. The decomposition of Subject 1 EDA signal. Sound stimuli are presented to the subject at moments denoted by colored vertical lines. In a), the amplitude of the observed EDA signal y is shown. In b), the EDA signal y ,after the difference matrix D is applied, is shown. In c), the recovered SCR events signal $\hat{x}$ is shown. In d), the reconstructed SCR component, computed as $h * x$,is shown.

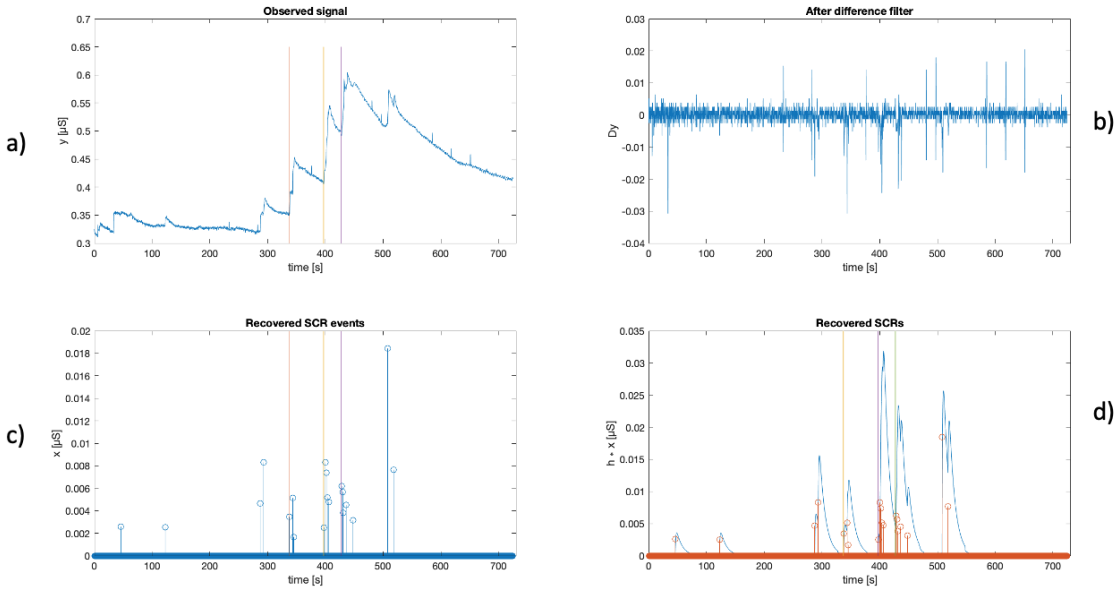

Figure 14. The decomposition of Subject 2 EDA signal. Sound stimuli are presented to the subject at moments denoted by colored vertical lines. In a), the amplitude of the observed EDA signal y is shown. In b), the EDA signal y ,after the difference matrix D is applied, is shown. In c), the recovered SCR events signal $\hat{x}$ is shown. In d), the reconstructed SCR component, computed as $h * x$,is shown.

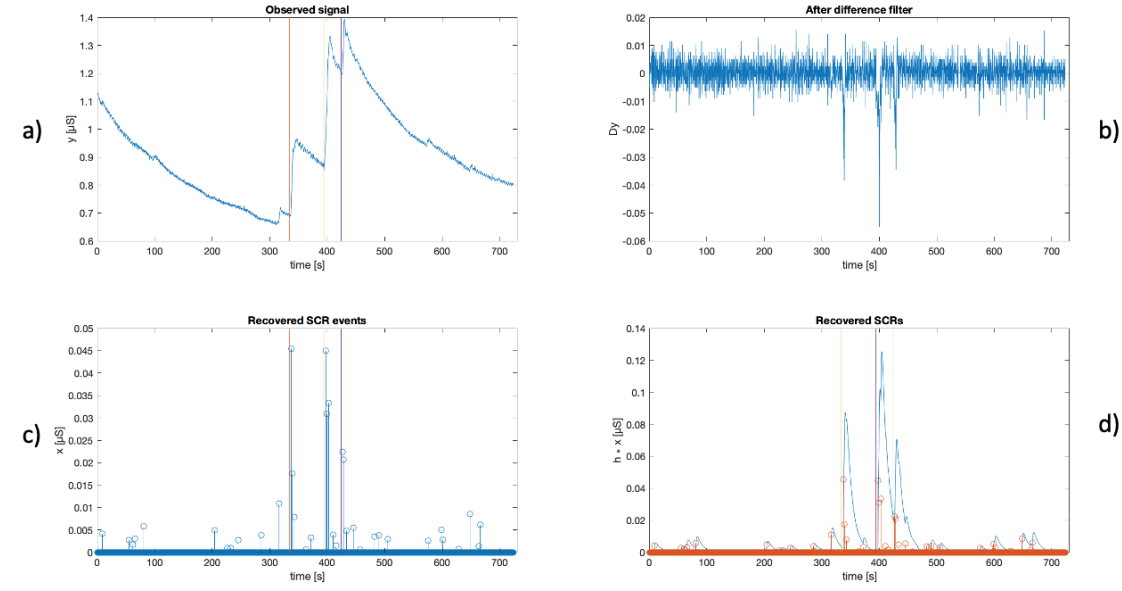

Figure 15. The decomposition of Subject 3 EDA signal. Sound stimuli are presented to the subject at moments denoted by colored vertical lines. In a), the amplitude of the observed EDA signal y is shown. In b), the EDA signal y ,after the difference matrix D is applied, is shown. In c), the recovered SCR events signal $\hat{x}$ is shown. In d), the reconstructed SCR component, computed as $h * x$,is shown.

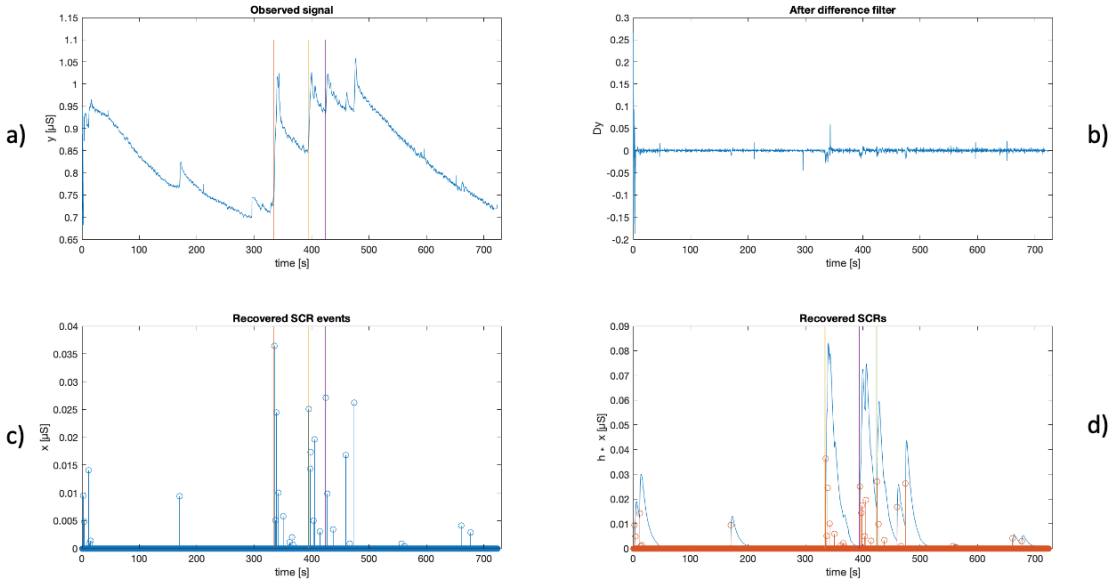

Figure 16. The decomposition of Subject 4 EDA signal. Sound stimuli are presented to the subject at moments denoted by colored vertical lines. In a), the amplitude of the observed EDA signal y is shown. In b), the EDA signal y ,after the difference matrix D is applied, is shown. In c), the recovered SCR events signal $\hat{x}$ is shown. In d), the reconstructed SCR component, computed as $h * x$,is shown.

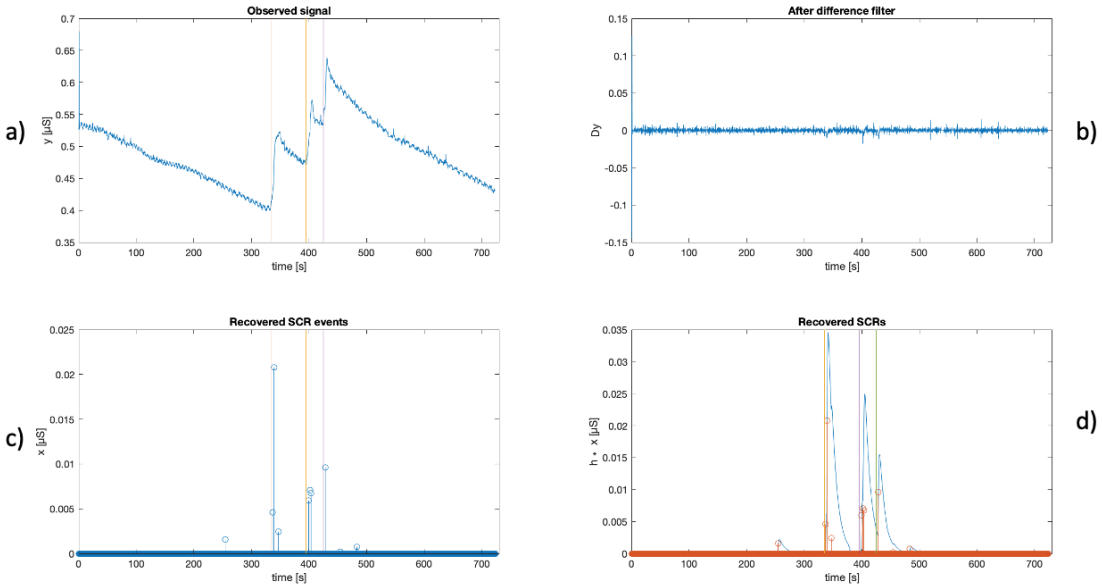

Figure 17. The decomposition of Subject 5 EDA signal. Sound stimuli are presented to the subject at moments denoted by colored vertical lines. In a), the amplitude of the observed EDA signal y is shown. In b), the EDA signal y ,after the difference matrix D is applied, is shown. In c), the recovered SCR events signal $\hat{x}$ is shown. In d), the reconstructed SCR component, computed as $h * x$,is shown.

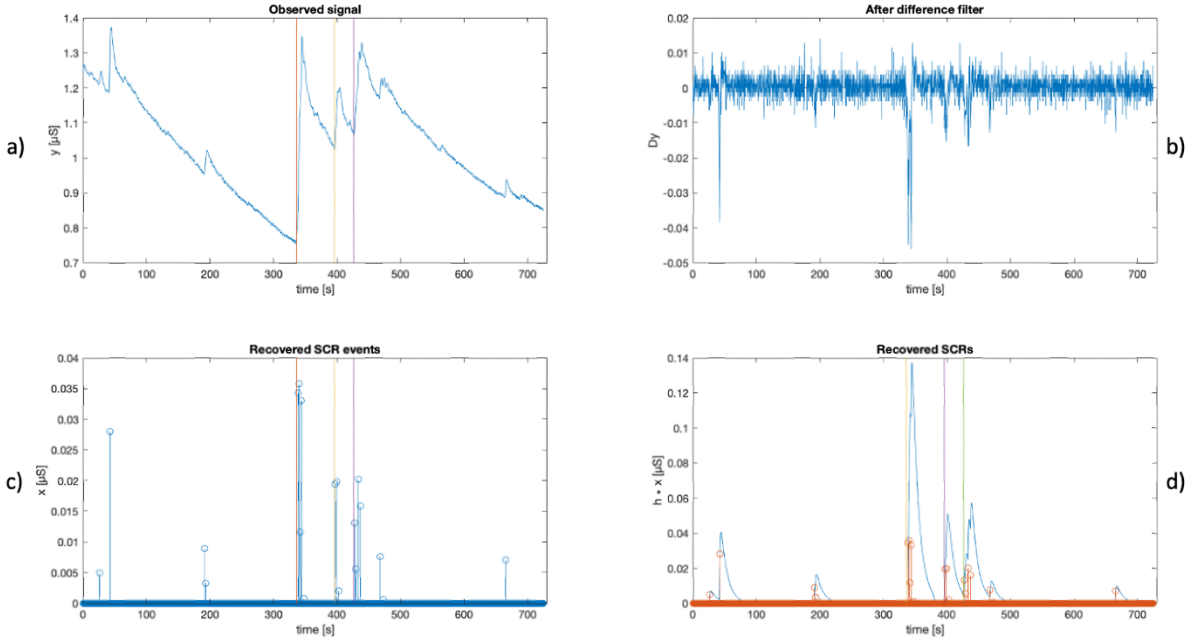

Figure 18. The decomposition of Subject 6 EDA signal. Sound stimuli are presented to the subject at moments denoted by colored vertical lines. In a), the amplitude of the observed EDA signal y is shown. In b), the EDA signal y ,after the difference matrix D is applied, is shown. In c), the recovered SCR events signal $\hat{x}$ is shown. In d), the reconstructed SCR component, computed as $h * x$,is shown.

5.2.2 SCR ONSET DETECTION RESULTS

In the Figures 19-20, a plot of the (Δ) LL-CS vector and (Δ) PG-CS vector for subject 1 is reported, respectively. The lengths of these vectors are equal to the number of time windows the EDA signal has been divided into, that is 68. The blue dots represent the vectors amplitudes in each time window.

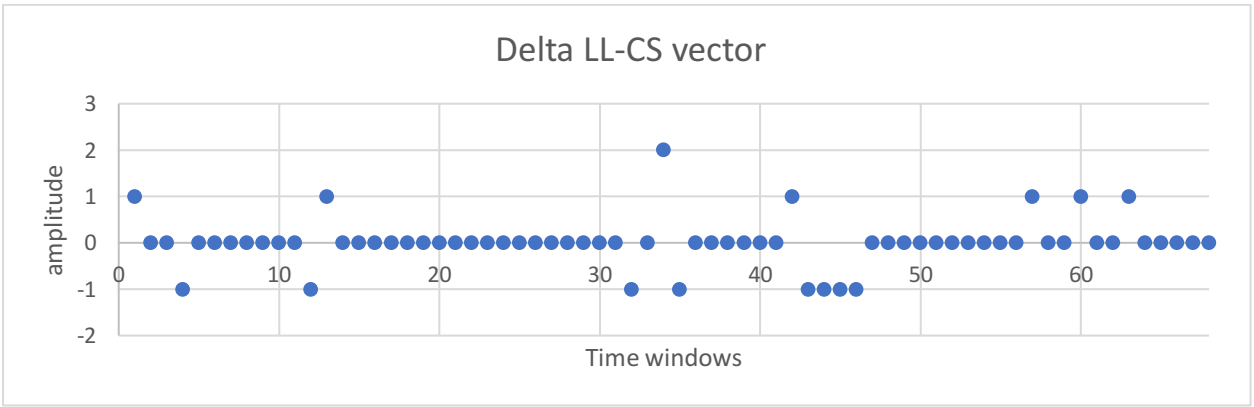

Figure 19. The plot of the Δ LL-CS vector with its amplitude in each time window represented by blue dot, for subject 1

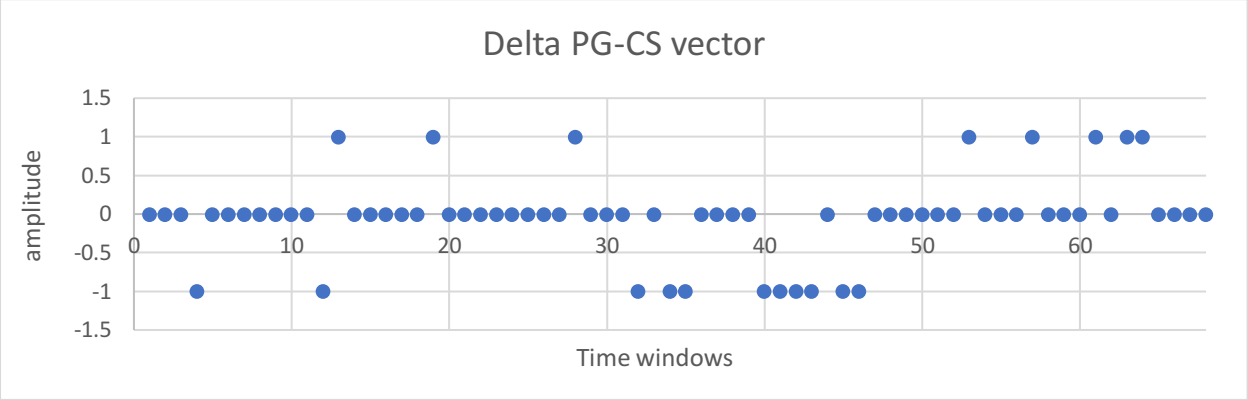

Figure 20. The plot of the Δ LL-CS vector with its amplitude in each time window represented by blue dot, for subject 1

In Figure 21, the global score (GS), expressed as a percentage, associated with each Δ vector, either LL-CS or PG-CS, is reported for every subject's EDA signal acquired. This score reflects the percentage of time windows where both Ledalab and CS-based approaches, or Pocket guide and CS-based approaches detect the same number of SCR onsets and can be interpreted as a measure of the CS approach ability in detecting SCR onsets compared to Ledalab approach or Pocket guide approach, both taken as gold standards.

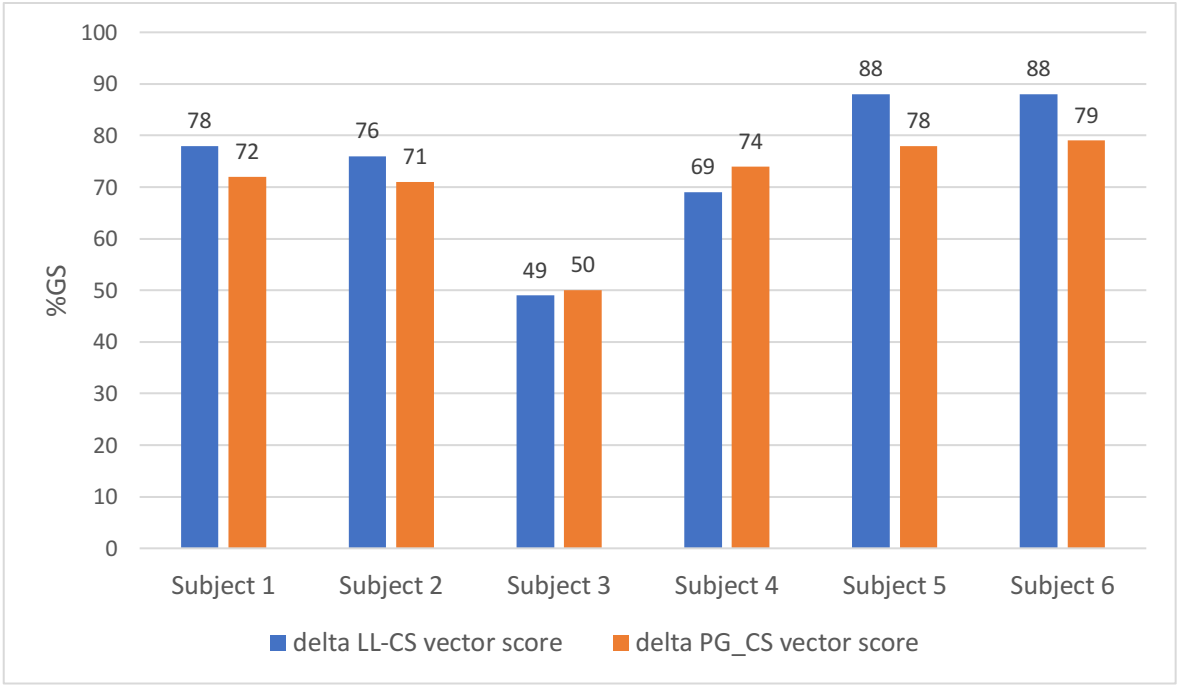

Figure 21. The histogram shows the percent global score associated to each Δ vector for every subject.

In Table 3 and Figure 22, and in Table 4 and Figure 23, the mean and standard deviation of the two Δ vectors, LL-CS and PG-CS, are reported for each subject.

Specifically, Table 3 and related Figure 22 correspond to an analysis carried out over all the 68 time windows which the reconstructed SCR events signal (in the case of the proposed approach), or the EDA signal (in the case of Ledalab or Pocket guide approach), are divided into; thus, Δ vectors length is equal to 68. Table 4 and related Figure 23 correspond to an analysis carried out only over 6 time windows, which are chosen around each sound stimulus.

Table 3. Mean and standard deviation (in brackets) of the Δ LL-CS and PG-CS vectors for each subject.

	SUBJECT 1	SUBJECT 2	SUBJECT 3	SUBJECT 4	SUBJECT 5	SUBJECT 6
Δ LL-CS vector	0(0,52)	0,06(0,57)	0,23(0,92)	-0,12(0,74)	-0,04(0,40)	0,15(0,40)
Δ PG-CS vector	-0,04(0,53)	-0,04(0,78)	-0,18(0,81)	-0,13(0,81)	0(0,51)	0(0,55)

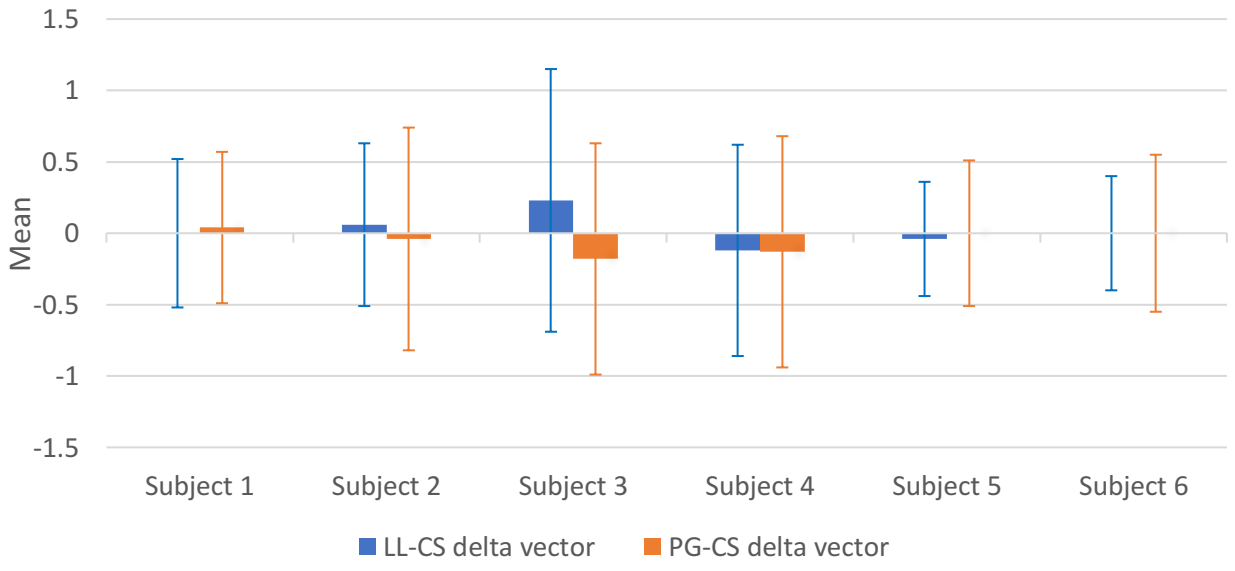

Figure 22. The boxplot shows the mean and standard deviation (as error bars) of the Δ LL-CS and PG-CS vectors for each subject.

Table 4. The mean and standard deviation (in brackets) of the Δ LL-CS and PG-CS vectors elements corresponding to time windows around the sound stimuli, for each subject.

	SUBJECT 1	SUBJECT 2	SUBJECT 3	SUBJECT 4	SUBJECT 5	SUBJECT 6
Δ LL-CS vector	-0,17(1,17)	-0,67(1,21)	-0,17(0,75)	-0,67(0,81)	-0,33(1,03)	-0,33(1,03)
Δ PG-CS vector	-0,83(0,40)	-1,83(1,17)	-0,67(1,21)	-1(1,55)	-0,67(1,03)	-0,67(0,81)

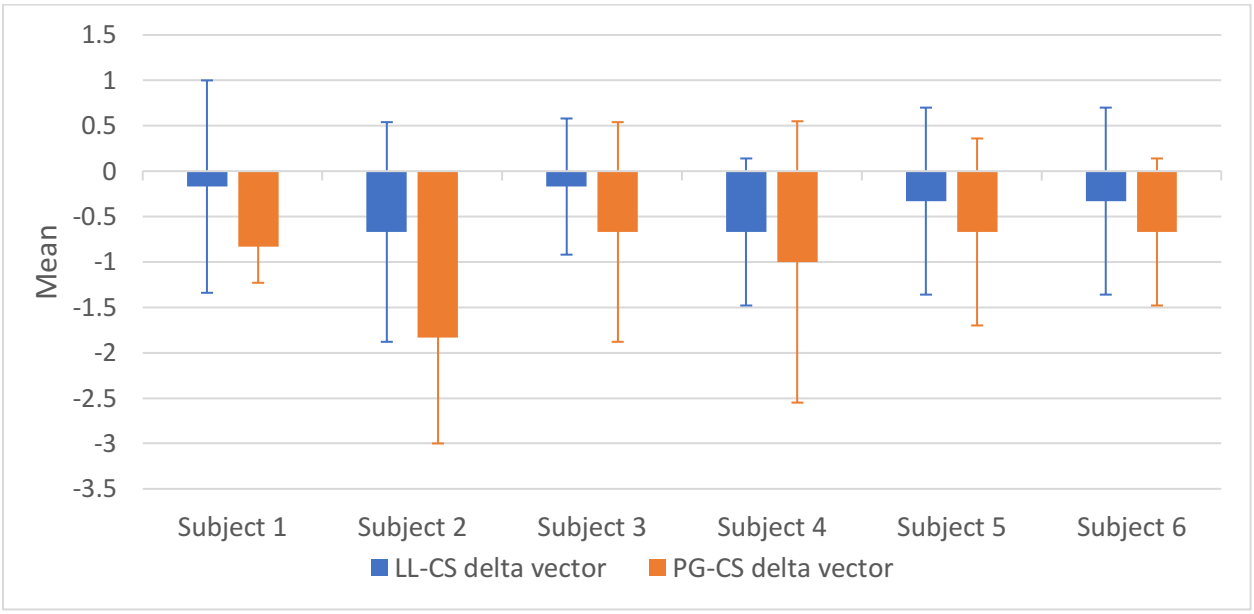

Figure 23. The boxplot shows the mean and standard deviation (as error bars) of the Δ LL-CS and PG-CS vectors elements corresponding to time windows around the sound stimuli, for each subject.

CHAPTER 6

DISCUSSION

In this work, a CS-based decomposition framework for EDA signals, as proposed by (jain), has been:

- implemented in Matlab with the associated convex optimization problem solved using CVX software;
- improved, with the addition of a post-processing step, in order to make the recovered SCR events signal both physiologically significant and as sparse as possible;
- tested, using a combination of both synthetically generated and experimentally acquired EDA data.

Moreover, once the sparse SCR events signals have been extracted from real EDA signals acquired during a sound stimuli experiment, by making the consistent assumption that each recovered SCR event corresponds to an SCR in the EDA signal, the SCR onsets detection ability of the CS-based approach has been tested against more traditionally used approaches such as the standard-trough to-peak analysis (TTP) available within the Ledalab tool [10], and the Pocket guide algorithm [11].

First, synthetically generated EDA data have been used to evaluate the feasibility and accuracy of the proposed CS based decomposition framework for several combinations of sparsity levels and energy levels [1]. The metric used to evaluate the accuracy of the CS based framework in recovering the SCR events signal is the recovery error [18]. As shown in Figure 11, it is possible to infer, from Panel a), that, in the case of a low amplitude baseline signal ($\alpha = 0.01$), the SCR events recovery ability of the CS approach depends uniquely on the number of SCR events inserted in the created EDA signal. This is an interesting result because it implies that, for synthetically generated EDA data, no matter what the number of baseline jumps is, for less than around 50 SCR events, the recovery error remains low (blue region) and thus the accurate recovery of the SCR events signal can take place. From Panel b) and c), instead, it is possible to note that, in the case of an increasing baseline amplitude ($\alpha = 0.1$ and $\alpha = 1$), the SCR events recovery ability of the CS approach depends significantly on the number of jumps present in the baseline signal, with the recovery error remaining low (blue regions) only in the case of few jumps.

This second result, which is found to be more appropriate in a situation of real EDA signal acquisition, assures the feasibility of applying the CS-based decomposition framework to our experiment addressing real EDA signals, since the EDA signal of each subject is acquired with the

person at resting condition, thus decreasing significantly the possibility of lots of movement artefacts causing discontinuities in the baseline signal.

Supported by these synthetic results, EDA signals have been acquired from 6 subjects during a sound stimuli experiment, as shown in Figure 12. The CS-based decomposition framework and post processing step are applied in order to extract the sparsest but physiologically meaningful SCR events signal and to reconstruct from it the phasic component of the original EDA signals, as shown in Figures 13-18. As it is possible to see in these figures, also simply by visual inspection of the original EDA signals, in addition to SCRs elicited by the 3 sound stimuli, there are several spontaneous or non-specific SCRs interspersed within the signal [11],[13]. Anyway, the CS-based decomposition framework is able to extract the SCR events and reconstruct the associated SCRs in both situations. As expected, there is a high density of recovered SCR events after each stimulus.

Moreover, by making the assumption that each SCR event corresponds to an SCR, and that the position of the $i-th$ SCR event in the SCR events signal vector corresponds to the position of the $i-th$ SCR onset, SCR onsets count metric is used to compare this approach to more traditional ones, such as Ledalab standard trough-to-peak detection analysis [10], and Pocket guide algorithm [11].

As shown in Figures 19-20, the focuses of this analysis are the Δ LL-CS and Δ PG-CS vectors whose elements represent the difference in the number of detected SCR onsets, in each time window which the EDA signal is divided into, between the Ledalab and CS-based approach and Pocket guide and CS-based approach, respectively.

As it is possible to see from Figure 21, the percentage of corresponding time windows sharing the same number of detected SCR onsets, is high between both the CS and Ledalab approach and CS-based and Pocket guide approach in most subjects. The scoring procedure assigns a positive score $(+1)$ to each delta vectors element based on the presence of the same number of detected SCR onset in the same time window. The problem with this strategy is that it does not take into account and does not penalize properly the setting where the variation in the number of SCR onsets detected in the same windows by the two methods is greater than 1.

To have an idea of this variation, the mean and standard deviation of both delta vectors are computed for each subject as shown in Table 3 and Figure 22, and Table 4 and Figure 23.

There are two possibilities, either the CS approach underestimates the number of SCR onsets in a time window compared to the other approaches, or it overestimates. From Table 3 and related Figure 22, it is possible to see that the mean of both delta vectors for every subject is very close to

zero, with the 68% of values in the delta vectors laying approximatively around -0.5 and $+0.5$ interval. In this case, it is still not clear which one of the two previously mentioned possibilities the CS-based approach falls into. By taking the mean and standard deviation of only subsets of delta vectors, more precisely the difference in the number of SCR onsets detected only in those time windows including or following a stimulus, the standard deviation increases: in this case, the 68% of values in the delta vectors lays approximatively in the mean ± 1 interval. Besides, a negative mean value for both delta vectors for all subjects, as shown in Table 4 and related Figure 23, relates to the fact that the CS-based approach systematically overestimates the number of SCR onsets in those time windows compared to the other two approaches, with a slightly less overestimation in the case of the Ledalab approach compared to the Pocket guide approach. Such a result is not necessarily tragic. A possible reason for such a performance of the CS-based approach compared to the other ones, could be attributed to its ability of detecting overlapping SCRs, an almost unsolved problem with most traditional analysis approaches. Further research in this direction is needed.

CHAPTER 7

CONCLUSION, LIMITATIONS AND FUTURE DEVELOPMENTS

In this work, a CS-based decomposition framework for EDA signals, as proposed by [1], has been Implemented in Matlab with the associated convex optimization problem solved using CVX software, improved with the addition of a post-processing step and tested using a combination of both synthetically generated and experimentally acquired EDA data. It is shown that with this approach, an accurate recovery of SCR events in both synthetically generated and experimentally acquired EDA measurement data occurs.

Moreover, starting from the sparse SCR events signal extraction as a result of the proposed decomposition, the SCR onsets detection ability of this CS-based approach has been tested against more traditionally used approaches such as Ledalab standard trough-to-peak analysis [10] and Pocket guide algorithm [11].

A limitation of this study results from the post-processing step which, if on one hand preserves the SCR events positions allowing then to test the SCR onsets detection of the proposed framework, on the other hand, does not entirely preserve SCR events amplitudes, therefore reconstructing a slightly different phasic component of the EDA signal. A way to overcome this problem would be to aggregate reconstructed the low amplitude SCR events around the maximum one found and chosen, instead of just discarding them. This consideration, along with a test on a larger population, is left for further research.

REFERENCES

[1] Jain, Swayambhoo & Oswal, Urvashi & Xu, Kevin & Eriksson, Brian & Haupt, Jarvis. (2016). A Compressed Sensing Based Decomposition of Electro-Dermal Activity Signals. IEEE Transactions on Biomedical Engineering. PP. 10.1109/TBME.2016.2632523.

[2] Posada-Quintero, Hugo & Chon, Kaye. (2020). Innovations in Electrodermal Activity Data Collection and Signal Processing: A Systematic Review. Sensors. 20. 479. 10.3390/s20020479.

[3] Critchley, Hugo & Elliott, Rebecca & Mathias, Christopher & Dolan, Raymond. (2000). Neural activity relating to generation and representation of galvanic skin conductance responses: A functional magnetic resonance imaging study. The Journal of neuroscience: the official journal of the Society for Neuroscience. 20. 3033-40.

[4] Garbarino, Maurizio & Lai, Matteo & Bender, Daniel & Picard, Rosalind & Tognetti, Simone. (2015). Empatica E3 - A wearable wireless multi-sensor device for real-time computerized biofeedback and data acquisition. 39-42. 10.1109/MOBIHEALTH.2014.7015904.

[5] Silveira, Fernando & Eriksson, Brian & Sheth, Anmol & Sheppard, Adam. (2013). Predicting audience responses to movie content from electro-dermal activity signals. UbiComp 2013 - Proceedings of the 2013 ACM International Joint Conference on Pervasive and Ubiquitous Computing. 707-716. 10.1145/2493432.2493508.

[6] Alexander, David & Johnston, P & Cooper, T & August, J.P. & Gordon, Evian. (2005). Separating individual skin conductance responses in a short interstimulus paradigm. Journal of neuroscience methods. 146. 116-23. 10.1016/j.jneumeth.2005.02.001.

[7] Benedek, Mathias & Kaernbach, Christian. (2010). Decomposition of skin conductance data by means of nonnegative deconvolution. Psychophysiology. 47. 647-58. 10.1111/j.1469-8986.2009.00972.x.

[8] Benedek, Mathias & Kaernbach, Christian. (2010). A continuous measure of phasic electrodermal activity. Journal of neuroscience methods. 190. 80-91. 10.1016/j.jneumeth.2010.04.028.

[9] Grant, Michael & SP, Boyd. (2014). CVX: MATLAB software for disciplined convex programming.

[10] "Ledalab MATLAB toolbox." [Online]. Available: http://www.ledalab.de/

[11] "EDA / GSR Pocket Guide - Imotions". Imotions, https://imotions.com/guides/eda-gsr/

[12] Cowley, Benjamin & Torniainen, Jari. (2016). A short review and primer on electrodermal activity in human computer interaction applications.

[13] Cacioppo, John & Tassinary, Louis & Berntson, Gary. (2007). Handbook of psychophysiology. 10.13140/2.1.2871.1369.

[14] Boucsein, Wolfram & Fowles, Don & Grimnes, Sverre & Ben-Shakhar, Gershon & Roth, Walton & Dawson, Michael & Filion, Diane. (2012). Publication recommendations for electrodermal measurements. Psychophysiology. 49. 1017-34. 10.1111/j.1469-8986.2012.01384.x.

[15] Topoglu, Yigit & Watson, Jan & Suri, Rajneesh & Ayaz, Hasan. (2020). Electrodermal Activity in Ambulatory Settings: A Narrative Review of Literature. 10.1007/978-3-030-20473-0_10.

[16] Candes, E.J. & Wakin, Michael. (2008). Wakin, M.B.: An introduction to compressive sampling. IEEE Signal Process. Mag. 25(2), 21-30. Signal Processing Magazine, IEEE. 25. 21 - 30. 10.1109/MSP.2007.914731.

[17] Eldar, Yonina & Kutyniok, Gitta. (2012). Compressed Sensing: Theory and Applications. 10.1017/CBO9780511794308.

[18] Salahdine, Fatima & Ghribi, Elias & Kaabouch, Naima. (2020). Metrics for Evaluating the Efficiency of Compressing Sensing Techniques. 10.1109/ICOIN48656.2020.9016490.

[19] Arie, Roi & Brand, Avraham & Engelberg, Shlomo. (2020). Compressive sensing and sub-Nyquist sampling. IEEE Instrumentation & Measurement Magazine. 23. 94-101. 10.1109/MIM.2020.9062696.

[20] Studer, Christoph & Baraniuk, Richard. (2011). Stable Restoration and Separation of Approximately Sparse Signals. Applied and Computational Harmonic Analysis. 37. 10.1016/j.acha.2013.08.006.

[21] "E4 Get Started Guide – Start Acquiring Physiological Signals". Empatica https://www.empatica.com/get-started-e4.

[22] Bradley, Magargaret M. and Peter J. Lang. "The International Affective Digitized Sounds (2nd Ediotion; IADS-2), Affective Ratings of Sounds and Instruction Manual Center for the Study of Emotion and Attention, 2007.